This is a public version of the accepted manuscript published in Applied Thermal Engineering.
http://10.1016/j.applthermaleng.2020.116487

Analysis of a hybrid dry cooling system for solar thermal electricity plants in deserts

Mario Biencinto*, Esther Rojas, Rocío Bayón
(*) corresponding author
Affiliation (all): Plataforma Solar de Almería. CIEMAT-PSA;
Address (all): Av. Complutense 40, 28040 Madrid (Spain)
Phone:+34 91 4962502, FAX : +34 91 3466037
e-mails: mario.biencinto@ciemat.es; rocio.bayon@ciemat.es , esther.rojas@ciemat.es

Abstract

This work analyses a new concept of hybrid dry cooling system composed of a latent heat storage module and an air-cooled condenser intended for solar thermal electricity plants located in desert locations with low water availability. This hybrid system is expected not only to improve the power block efficiency but also to reduce parasitic consumptions of air-cooled condensers, taking advantage of the temperature oscillations in such locations. For evaluating those advantages, a simulation model of a solar thermal plant that includes either conventional dry or hybrid cooling system has been developed with TRNSYS, so that both approaches can be compared. The annual behaviour of the corresponding plants in terms of electricity production has been simulated for various desert locations, different cooling system configurations and two phase change materials (PCM) for the latent module: RT35HC and Paraffin C21, with melting temperatures of 35 ºC and 40 ºC, respectively. Also, suitable operation strategies have been evaluated in order to optimize the performance of the hybrid cooling concept. Simulation results show that an increase in net electricity from 0.3% to 0.6% for Paraffin C21 or from 0.1% to 0.5% for RT35HC could be obtained per year if a hybrid cooling system is used. The use of a PCM with higher melting points such as Paraffin C21 seems to provide better results in terms of net annual production, particularly in locations with high ambient temperatures at night (like Abu Dhabi or Aswan). Although issues like electricity prices, financial and equipment costs should also be considered, a preliminary economic analysis shows that the cost-to-latent heat ratio of the PCM should be below $4.5 \cdot 10^{-3}$ €/kJ to enable the feasibility of the proposed concept

Keywords: *hybrid dry cooling; latent heat storage; solar thermal electricity; phase change material; air-cooled condenser; simulation model*

Nomenclature

A	heat exchange area, m^2
A_c	net collection area, m^2
C	heat capacity rate, W/K
c_p	specific heat capacity, J/(kg·K)
C_r	heat capacity ratio, -
D	diameter, m
f	Darcy friction factor, -
F	proportionality factor, -
G_b	direct normal solar irradiance, W/m^2
h	specific enthalpy, J/kg
$K(\theta)$	incidence angle modifier, -
L	length, m
m	mass, kg
$\dot{m}$	mass flow rate, kg/s
p	pressure, Pa
$\dot{Q}$	thermal power, W
Q	thermal energy, J
Re	Reynolds number, -
t	time, s
T	temperature, ^oC or K
U	heat transfer coefficient, $W/(m^2 \cdot K)$
v	velocity, m/s
w	specific work, J/kg
W	electric energy, MWh
$\dot{W}$	electric power, W

Acronyms

ACC	air-cooled condenser
Conv-DC	conventional dry cooling
DNI	direct normal solar irradiance (equivalent to G_b)
Hy-DC	hybrid dry cooling
HX	heat exchanger
ITD	initial temperature difference
LHS	latent heat storage
LMTD	logarithmic mean temperature difference
NTU	number of transfer units
PB	power block
PCM	phase change material
PSA	Plataforma Solar de Almería
SF	solar field
STE	solar thermal electricity
TTD	terminal temperature difference

Greek symbols

Δ	increment or variation
ε	effectiveness, -
η	efficiency or performance factor, -
θ	incidence angle, ^{o}
ρ	density, kg/m^3

Abbreviations in subscripts

amb	ambient

cond	condenser
ext	turbine extraction
gener	electric generator
gross	gross electric power
loss	thermal or electric losses
m	electro-mechanical
max	maximum
melt	melting
min	minimum
net	net electric power
no-sh	non-shared-flow strategy
oper	operation
opt,0º	peak optical
ref	reference or threshold value
s	isentropic
sh	shadowing factor or shared-flow strategy
turb	turbine
u	useful

1. Introduction

In Solar Thermal Electricity (STE) plants, sunrays are concentrated with the help of mirrors to heat up a fluid, which is driven to a power block that generates electricity by means of a thermodynamic cycle. Up to date, STE comprises almost 10 GW_e operational, under construction or in development worldwide [1]. Like any other power plant based on a thermodynamic cycle, these plants require large amounts of water (from 2460 to 3760 m^3/GWh [2]) for power-block cooling [3], make-up water and generation of sealing steam. Additionally, STE plants require some water for cleaning of solar collectors' mirrors, but the water amount for such cleaning is below 5% of the above figures. Since electricity production of STE plants is directly proportional to the annual amount of local direct normal solar irradiance (DNI) and the highest DNI values are found in arid or desert areas, saving water strategies are major issues for a STE plant to be constructed in those locations.

To reduce water consumptions in STE plants, different dry-cooling systems for the power block have been proposed and implemented [4]. Overall, two main configurations are distinguished in dry-cooling systems [5]: direct and indirect. In the direct configuration, the exhaust steam from the turbine outlet is driven to an air-cooled condenser (ACC) where the latent heat is released to the ambient air. In the indirect configuration, the outlet steam from the turbine is condensed through a conventional wet-cooling condenser by using a secondary water circuit. The water is then cooled down by an air-cooled heat exchanger or a cooling tower. Hence, in this case the dry cooling applies only to the secondary circuit.

Hybrid cooling systems are expected to combine one or both of the aforementioned solutions, direct or indirect, with additional devices or technologies to improve the performance of the cooling process or to reduce water consumptions. The approach of using hybrid cooling systems in indirect configuration has been addressed in previous works, either with air-cooled heat exchangers [6][7] or with natural draft cooling towers [8][9]. In addition, the EFCool project [10] analysed an indirect hybrid cooling system with latent storage to support the heat exhaustion of a cooling tower. In contrast, the present study focuses on a hybrid dry cooling concept in direct configuration. This concept, initially proposed by Pistocchini and Motta [11], consists in using an ACC combined with a latent heat storage (LHS) system. The LHS accumulates all or part of the exhaust heat from the turbine during the day time in order to delay its release to the night time, when lower ambient temperatures are expected. This should not only reduce ACC fan power consumption, but also

improve the overall performance of the power block because condensation temperatures would be lower than the used with a conventional ACC system. The combination of ACCs with novel LHS systems has been analysed theoretically in [12], for instance.

The latent storage proposed for the hybrid cooling system contains a phase change material (PCM) with a melting temperature similar to the condensation temperature of the turbine exhaust steam. However, we must keep in mind that LHS systems with PCMs pose important challenges regarding the heat transfer in storage devices. The low thermal conductivity of PCMs used in low-medium temperature applications implies low heat transfer coefficients, which dramatically increases the heat exchange area required to provide reasonable heat transfer rates. In order to improve the heat transfer in LHS systems, several solutions such as finned tubes [13][14][15], composite materials [16][17] or PCM encapsulation [18][19] have been proposed and investigated. Unlike these works, both the study of Pistocchini and Motta [11] and the one presented here focus on the theoretical benefits of the hybrid cooling system for a STE plant in terms of electricity production, assuming that the LHS system works ideally and hence the concept is feasible from the technical point of view.

According to Pistocchini and Motta study [11], the potential of the hybrid concept is bound to the daily variations in ambient temperature, which did not seem to be large enough in the specific location considered in their work. This made the storage regeneration a critical issue because it required significant parasitic consumptions and imposed a lower limit to the condensing temperature. However, in their study they considered only one operation strategy, either in charge or discharge processes. During the day time, the LHS was always operated in parallel to the ACC, whereas during the nighttime the discharging strategy was always aimed to regenerate completely the LHS. As a result, they conclude that this cooling concept would be feasible only if PCM costs were very low.

To our opinion, the charging strategy considered in their work leads to a modest reduction in the condensing temperature compared to the individual charging of the LHS; while the discharging strategy may involve important parasitic consumptions in the hottest nights of the year. Therefore, a further analysis in terms of STE plant location and operating strategies has been performed in the present work. On the one hand, various deserts with very different daily temperature intervals and ranges have been considered for the STE plant locations. This would help determine for which ones the hybrid cooling approach is more interesting. On the other hand, the present study considers operation strategies specifically designed to take advantage of the behaviour of STE plants. In this way, various strategies concerning the sharing of turbine exhaust steam between the LHS and the ACC are proposed and evaluated in order to see whether the annual electricity production of a STE plant can be increased. The impact of LHS regeneration at night and its effect on parasitic consumptions have been analysed as well.

For the case of the LHS system, an ideal device is considered regarding the heat transfer mechanism between the water/steam and the PCM. In contrast to the study of Pistocchini and Motta [11], the PCMs considered have been previously tested in order to check the occurrence of supercooling or incongruent phase change phenomena.

The advantages of this concept have been evaluated by comparing the annual electricity production of STE plants that use either hybrid or conventional dry cooling systems with the help of a simulation model. The STE plant considered in the model includes a solar field with parabolic-trough collectors, a two-tank thermal storage system and a power block with 55 MW_e gross electric power, equivalent to the gross output of most commercial STE plants in Spain. The complete model for this STE plant is developed in TRNSYS and it is applied for simulating the annual plant behaviour for different desert locations, cooling system configurations and strategies. The resulting annual production values for the different cases are compared and discussed. In addition, some guidelines are suggested regarding operation strategies and expected economic feasibility of the proposed concept.

This work is structured as follows: section 2 describes the STE plant and the hybrid cooling system; section 3 explains the modelling approach adopted; section 4 shows the results obtained from the simulations, including an example of daily results to describe the hybrid cooling system behaviour, annual results for each desert location and configuration and a preliminary economic evaluation; finally, overall conclusions are presented in section 5.

2. STE plant description

The STE plant considered for the simulation model is an Andasol-type plant. Andasol plants [20] are representative examples of the commercial STE plants with thermal storage located in Spain. This choice is supported because the simulation model applied in this work has been already validated with data of real STE plants of this type [21][22]. A schematic diagram of this plant is depicted in Figure 1, in which the cooling system for the turbine exhaust proposed in this work has been included.

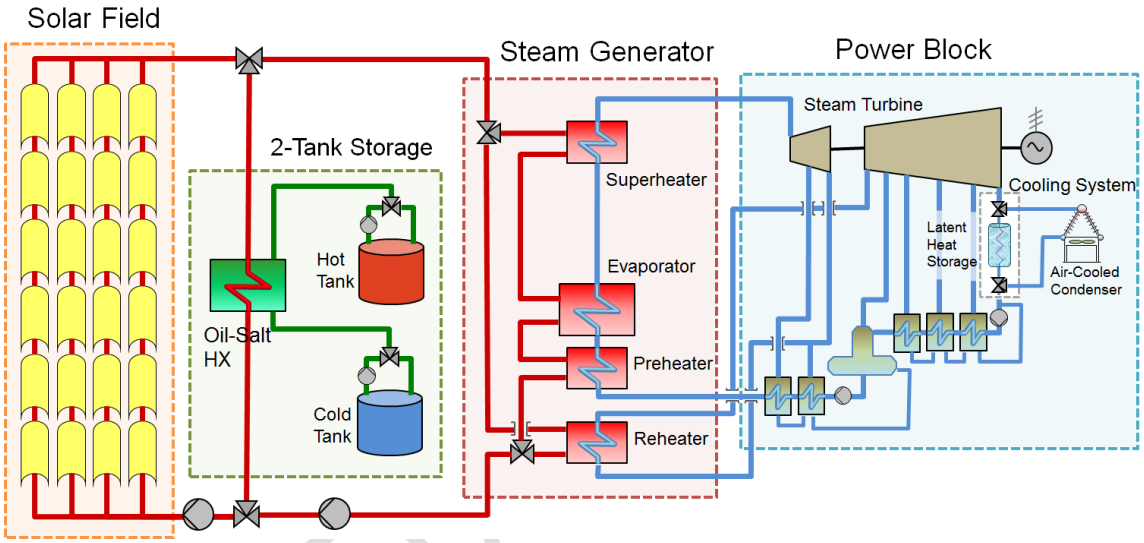

Figure 1: Schematic diagram of the STE plant considered in the simulation model

The plant includes a solar field of parabolic-trough collectors with thermal oil as heat transfer fluid, a two-tank storage system with molten salts and a power block based on a steam Rankine cycle. The solar field is composed of 156 loops with 6 EuroTrough-type collectors 100 m long each and the heat transfer fluid is Dowtherm®-A thermal oil. The storage system has 1 GWh capacity, i.e. around 7.5 h generation at nominal conditions, and the solar salt mixture (60wt% $NaNO_3$/40wt% KNO_3) as storage medium. A heat exchanger is used to transfer the thermal energy between the heat transfer fluid and the molten salt. The power block consists of a reheat steam Rankine cycle of 55 MW_e gross electric power with 6 turbine steam extractions, including 5 feed-water heaters and a deaerator. A steam generation train, comprising preheater, evaporator, superheater and reheater, connects the solar field to the power block.

The main features and working parameters of this STE plant are gathered in Table 1.

Table 1: Main features and working parameters of the STE plant considered in the simulation model

Parameter	Value
Working fluid in receiver tubes	Dowtherm® A
Type of solar collector	EuroTrough
Aperture width (m)	5.76
Focal length (m)	1.71

Net collection area for each collector (m^2)	548.35
Total length of receiver tube for each collector (m)	98.7
Outer diameter of the metal receiver tube (m)	0.07
Inner diameter of the metal receiver tube (m)	0.065
Peak optical efficiency (%)	76.5
Cleanliness factor of the mirrors (%)	97
Distance between collector rows (m)	16.5
Number of collectors per loop	6
Number of loops in the solar field	156
Net collection area of the solar field (m^2)	513256
Nominal temperature at collectors' loop outlet (ºC)	393
Nominal temperature at collectors' loop inlet (ºC)	296
Nominal pressure at collectors' loop inlet (Pa)	$2.7 \cdot 10^6$
Fluid in the 2-tank storage system	Solar Salt
Size of the 2-tank storage system (t)	25500
Efficiency of HXs and steam generator (%)	99
Nominal gross efficiency of the power block (%)	39.5
Nominal gross electric power (MW_e)	55
Nominal steam temperature at condenser inlet (ºC)	38
Nominal steam pressure at condenser inlet (Pa)	6630
Nominal steam mass flow rate at condenser inlet (kg/s)	38.9

Two versions are considered for the cooling system of the power block (see Figure 1): a conventional dry cooling (Conv-DC) based on an ACC and a hybrid dry cooling (Hy-DC) that combines an ACC with a LHS module. In Figure 1, the LHS tank in parallel to the ACC is shown within a dashed rectangle to represent both cooling versions. The working principle of the Hy-DC system is described below.

2.1. Hybrid dry cooling system (Hy-DC)

The LHS module of the Hy-DC is connected in parallel to the ACC. This system is arranged in direct configuration, which means that the steam from turbine outlet is condensed in the ACC and/or LHS module without using a secondary water circuit. LHS module should accumulate all or part of the exhaust heat from the turbine during the day time in order to delay its release to the night time, when lower ambient temperatures are expected. This module consists of a container filled with a PCM whose melting temperature should be similar to the saturation temperature of the steam to be either condensed (in LHS charge) or evaporated (in LHS discharge).

The charging process of the Hy-DC system is displayed in the scheme of Figure 2. During a charging process, exhaust heat from turbine output is delivered to the LHS and/or to the ACC by means of a three-way control valve, depending on ambient temperature and LHS state. The PCM, initially in solid phase, absorbs the released energy from the steam condensation and becomes liquid. Since steam condensation through the LHS system avoids the ACC operation, charging processes are expected to be scheduled at the hottest hours of the day, when ACC parasitic consumptions become higher and maximum power savings can be obtained.

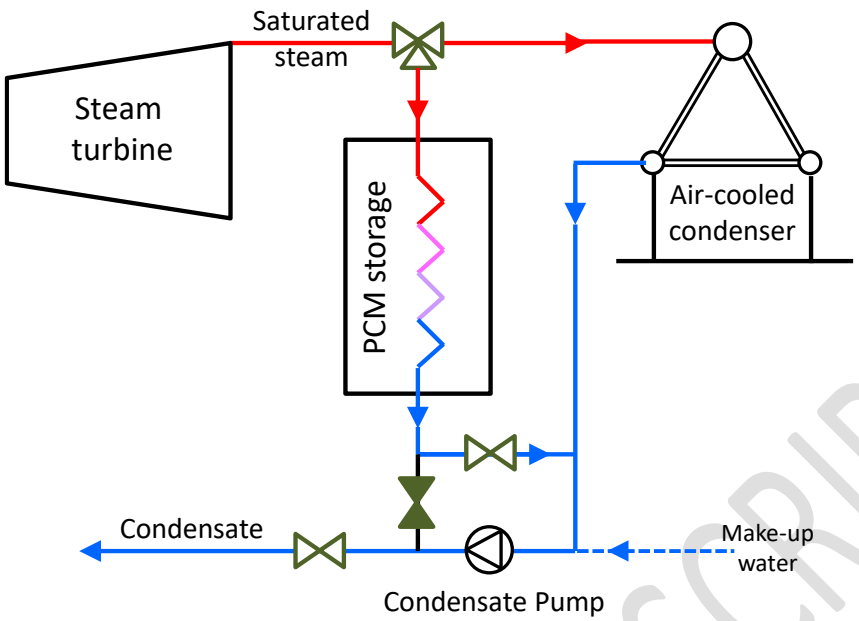

Figure 2: Charging process of the hybrid dry cooling system

During the night-time, when the steam turbine is not working, discharge process can be carried out (see Figure 3) by circulating liquid water through the LHS. The heat stored in the LHS module is released by producing low temperature steam which is further condensed with the help of the ACC. Since ambient temperatures at night are commonly lower than during daytime, the power consumed by the ACC fans is therefore reduced.

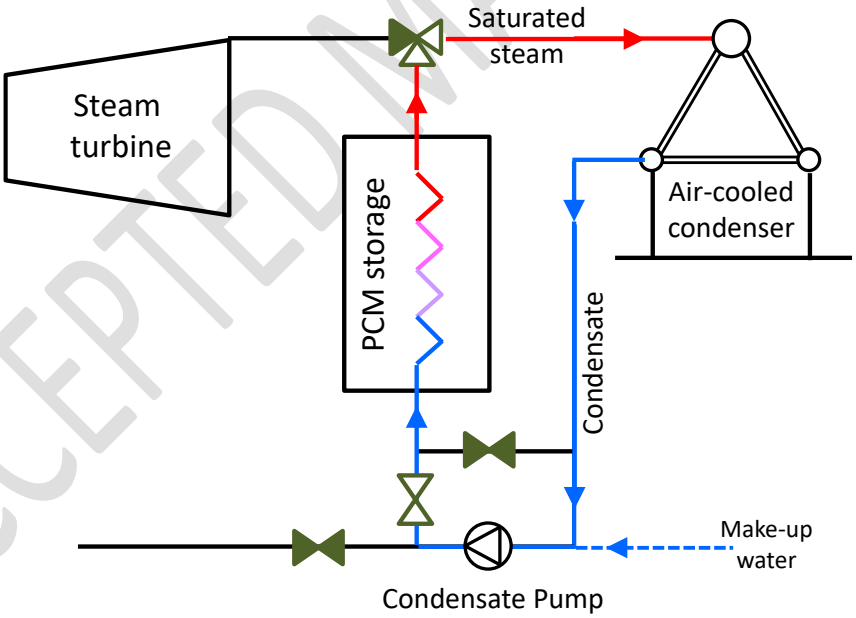

Figure 3: Discharging process of the hybrid dry cooling system

An Andasol-type STE plant in a desert location is expected to operate in a sunny summer day for about 12 h with solar-only support. On the other hand, the plant operation from the storage system can be performed at reduced output, this means that the 7.5 h established at nominal conditions are usually extended up to 8 or even 9 h. This leads to more than 20 h operation of the power block, leaving a window of 3 to 4 h of plant shutdown. For simplicity, LHS module will be discharged when turbine is not under operation and therefore 3 h storage capacity has been chosen for the LHS in order to ensure its regeneration.

The selection of the PCM for the LHS relies on the most likely ambient temperature at the plant location. To evaluate how the use of PCM with different melting points can affect the system performance, two commercial products have been considered: RT35HC [23], with a melting temperature of 35 ºC, and Paraffin C21 [24], with a melting temperature of 40.2 ºC.

The thermophysical properties of these PCMs reported in the literature and relevant for this application are summarized in Table 2. For the case of RT35HC some preliminary assessment tests consisting in thermal cycling have been previously performed in our laboratory [25].

Table 2: Thermophysical properties of the PCMs selected for the LHS module

Property	RT35HC	Paraffin C21
Melting Temperature (ºC)	35 [23]	40.2 [26]
Density of solid phase (kg/m^3)	860 [23]	930 [27]
Density of liquid phase (kg/m^3)	770 [23]	830 [27]
Thermal conductivity (W/(m·K))	0.20 [23]	0.21 [27]
Phase Change Enthalpy (kJ/kg)	240 [23]	159 [26]

2.2. Locations and meteorological data

In order to analyse the system behaviour for different geographic coordinates and meteorological conditions, 7 locations corresponding to desert or arid areas in various continents have been selected for this study. The geographic coordinates, annual direct solar radiation and yearly ranges of ambient temperature for such locations are summarized in Table 3. Hourly meteorological data for typical years, including DNI and ambient temperature, are available from different sources [28][29][30] to conduct the foreseen simulations.

Table 3: Geographic coordinates and main annual meteorological data of the considered locations

Location	Latitude (º N)	Longitude (º E)	*DNI* (kWh/m^2)	T_{amb} *max.* (ºC)	T_{amb} *min.* (ºC)
PSA, Almería, Spain [28]	37.09	-2.36	2071.5	43.0	0.7
Ouarzazate, Morocco [29]	30.93	-6.9	2636.0	38.1	-2.9
Abu Dhabi, UAE [30]	24.43	54.65	2294.9	47.0	5.0
Aswan, Egypt [30]	23.97	32.78	2433.5	44.8	7.4
Tonopah, USA [30]	38.07	-117.13	2422.2	36.7	-16.7
Las Vegas, USA [30]	36.08	-115.17	2606.6	44.4	-4.4
Sevilla, Spain [30]	37.42	-5.9	1772.7	43.0	-2.0

It is worth mentioning that the PCMs proposed for the LHS module (RT35HC and Paraffin C21) have melting temperatures near the maximum ambient temperatures expected in the different locations here considered.

3. Modelling approach

The simulation model for the STE plant has been implemented within the TRNSYS software environment [31]. Overall, it is based on the model described in previous works [21][32][33], but it incorporates additional components to simulate the proposed dry and hybrid cooling systems (Conv-DC and Hy-DC) so that both options can be compared.

The basic algorithm for the calculations performed in the simulation model is displayed in the simplified flow chart of Figure 5. This algorithm can be applied to both versions of the cooling system by ignoring the LHS

in the case of the Conv-DC configuration.

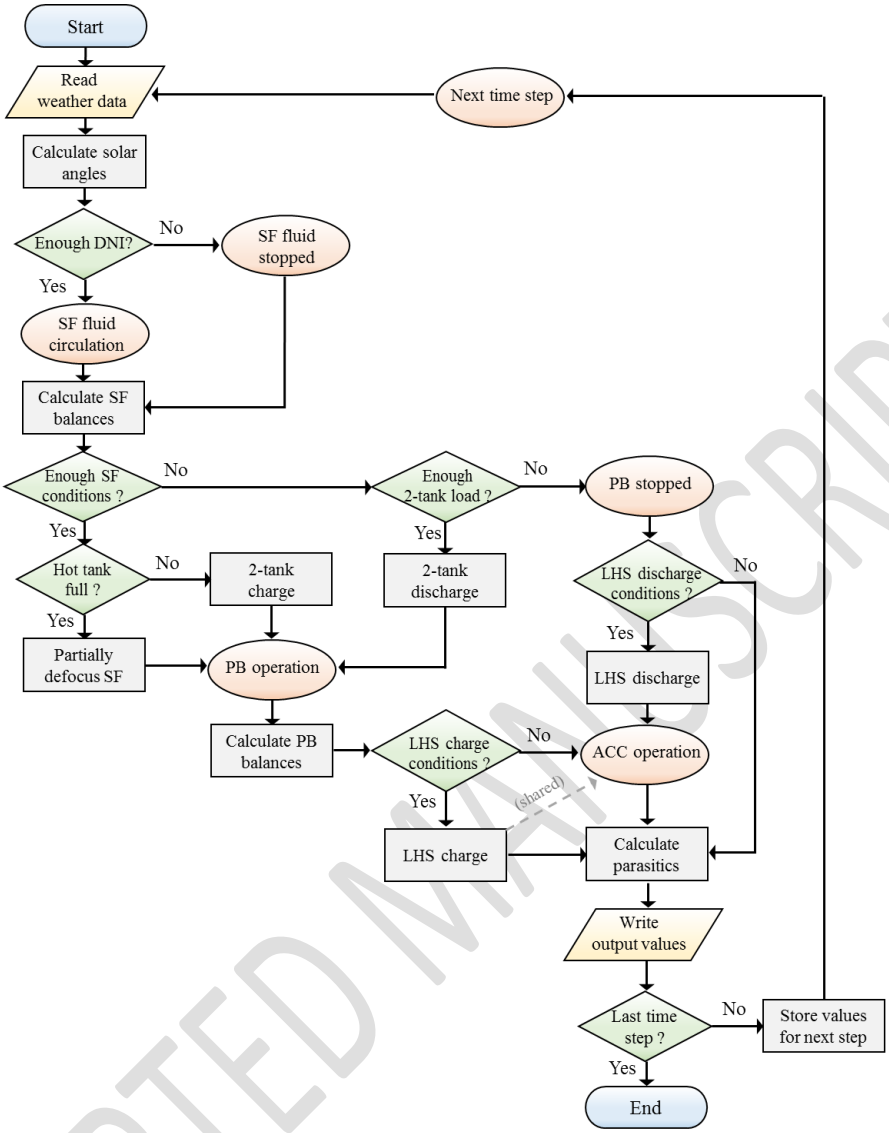

Figure 4: Simplified flow chart of the calculations performed in the STE plant simulation model

As seen in Figure 5, weather data are read from the input file to perform the corresponding calculation of solar angles (zenith angle, incidence angle on solar collectors). When the DNI is above a minimum value (100 W/m^2), the thermal oil is circulated through the solar field, calculating thermal and hydraulic balances with the SF model for dynamic flow conditions. Otherwise, there is no fluid circulation in the SF and energy balances are calculated for static flow. If the fluid in the SF has enough temperature to run the power block (T_{out} > 320 ºC), the PB is operated and the remaining flow is sent to charge the 2-tank storage system. When the hot tank is full it cannot be further charged, causing a partial defocusing of the SF in the subsequent time step. In case the SF conditions are not sufficient to operate the PB and there is enough storage load, the hot salt tank is discharged to complete the SF support and thus allow the PB operation.

In the Hy-DC configuration, the PB operation leads to the LHS charging whenever certain conditions occur. The specific conditions to charge the LHS system depend on the operation strategy and are established and discussed in section 3.5. On the other hand, when the PB is stopped and the LHS discharge conditions (also explained in section 3.5) are given, the LHS system is discharged to the environment by means of the ACC. Both the LHS discharging and the PB operation without LHS charging involve the use of the ACC. Moreover,

the charging process of the LHS with shared heat rejection (represented with a dashed grey arrow in Figure 5) also requires the operation of the ACC. Finally, the calculation of parasitic consumptions enables obtaining net electric power from gross electric power.

The main results of the simulation are recorded in an output file each time step. The simulation either continues by reading weather data for the next time step or ends when the last time step is attained.

The general layout of the TRNSYS model that implements the described algorithm is depicted in Figure 5, including equation editors, components from the standard TRNSYS library (for instance, to read input data or determine solar angles) and components developed in-house to simulate specific elements and subsystems of a STE plant. Some macro-components shown in Figure 5, containing in turn several components, model the main plant subsystems such as the solar collectors' loop or the storage system.

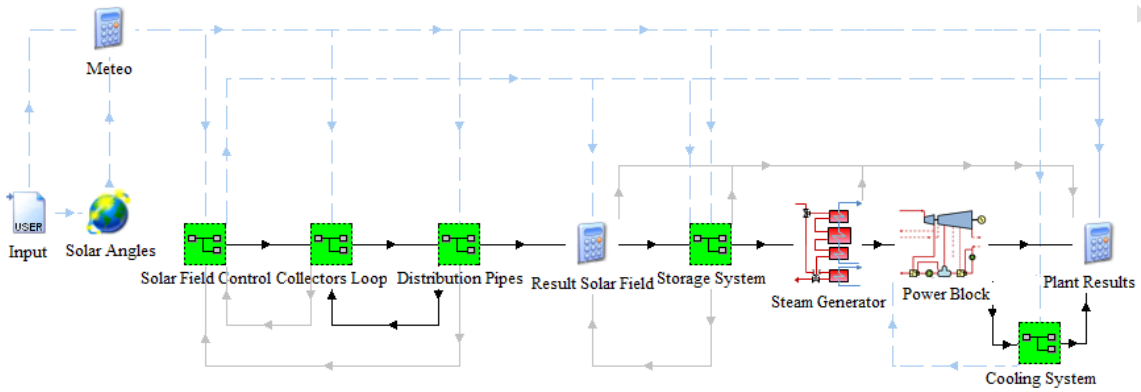

Figure 5: Screenshot of the TRNSYS model for the STE plant

The following sections describe the modelling approach adopted for the different subsystems of the plant, paying special attention to the cooling system in two versions (Conv-DC and Hy-DC) and its operation strategy. Since the model of solar field, storage system and power block for a STE plant is thoroughly explained in previous works [21][22][33][34], those subsystems are only described in brief. Nevertheless, a summary of the main equations and assumptions considered in the simulation model is included in Appendix A.

3.1. Solar field and two-tank storage system

The solar field model is performed by the simulation of one collector loop, since the input variables (solar radiation, ambient temperature, flow, etc.) to every loop are all equal. The result is then multiplied by the total number of loops to obtain the useful power for the entire solar field. Basically, a stationary approach is followed to determine the thermal power yielded by the solar field at nominal conditions. Nevertheless, during non-stationary conditions, such as transient clouds, startup and shutdown processes, energy balances regarding thermal inertia are applied to estimate the evolution of temperatures.

The solar field in the simulation model is basically built upon two TRNSYS components: parabolic-trough solar collector and insulated pipe. In general terms, the thermal model of PT collectors is performed by evaluating the useful power gained by the fluid with an energy balance between solar power absorbed by the system and thermal losses to the environment. EuroTrough-II collectors [35] with SCHOTT PTR®70 receiver tubes [36] are here considered.

The hydraulic model for both receiver tubes and connecting pipes is based on the evaluation of pressure drop through straight pipes and accessories using the Darcy-Weisbach equation [37], establishing the friction factor according to the turbulence regime of the fluid. The calculation of pressure losses enables the evaluation of

pumping consumptions, which will be added to the rest of parasitic consumptions of the plant.

The two-tank storage system is implemented by means of a component that models each molten salt tank as a storage tank with variable volume. The model of the storage system is completed by including piping, operation mechanisms and an oil/salt heat exchanger. This heat exchanger, which transfers the useful energy from the solar field to the storage system, is modelled by using the Number of Transfer Units (NTU) method [38].

3.2. Steam generator and power block

The model for the steam generation train, which represents the connection between the solar field and the power block, is implemented with a component that applies the NTU method to each of its elements: preheater, evaporator, superheater and reheater.

The model of the power block analyses the system behaviour in both nominal and part-load conditions using the Spencer-Cotton-Cannon method [39]. The methodology is based on similar studies [40] for typical Rankine cycles used in STE plants, also applying the NTU method to calculate heat transfer coefficients and temperature differences in feedwater heaters and the deaerator.

The steam parameters at the turbine outlet constitute the inputs for the cooling system model. Specifically, the mass flow rate of steam, $\dot{m}_{steam}$, and the enthalpy difference between the outlet steam and liquid water, $\Delta h_{steam,cond}$, enable the calculation of the thermal power to be exhausted through the condenser (i.e., by the cooling system):

$$\dot{Q}_{cond} = \dot{m}_{steam} \Delta h_{steam,cond} \qquad (1)$$

Sections 3.3 and 3.4 describe the specific approach adopted to model the cooling system considered to exhaust that thermal power, either in the Conv-DC or in the Hy-DC configuration.

3.3. Conventional dry-cooling system (Conv-DC)

Most commercial STE plants using dry cooling systems operate with variable steam pressure at the turbine outlet, that is, at the condenser inlet. The steam pressure in the condenser is established according to the ambient temperature in order to use reasonable values of air mass flow rate through the ACC fans and hence to maintain an almost constant parasitic consumption of the cooling system [41]. This is the approach adopted here in the Conv-DC system model.

Figure 6 displays the working principle of an ACC used for cooling the exhaust of a steam turbine. The scheme on the left (a) shows the water and air flows involved and the heat-temperature diagram on the right (b) the relationships between their temperatures. Liquid water and steam flows are represented with solid lines (blue and red, respectively), whereas air flow is displayed with dashed green line.

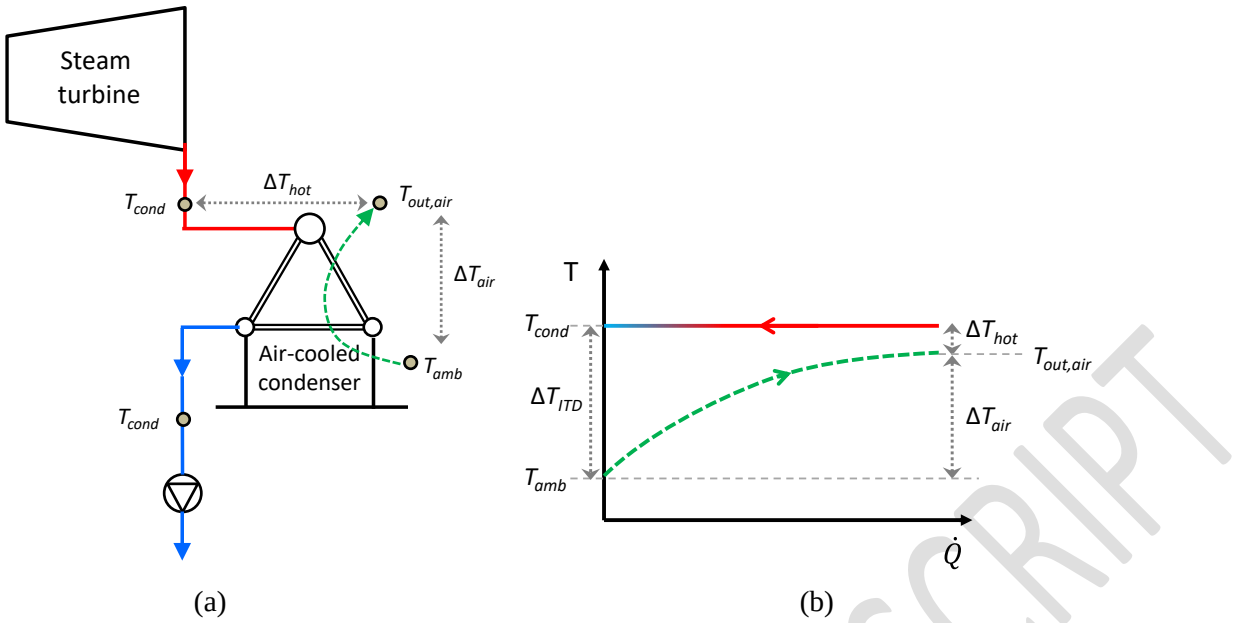

Figure 6: Working principle of an ACC used for cooling the exhaust of a steam turbine. (a) Scheme showing inlet/outlet flows of water and air. (b) Associated heat-temperature diagram

The main design parameter of an ACC is the initial temperature difference (ΔT_{ITD}). According to the diagram of Figure 6(b), $\Delta T_{ITD} = \Delta T_{air} + \Delta T_{hot}$, where ΔT_{air} is the temperature rise of the ambient air and ΔT_{hot} the temperature difference at the hot side of the ACC. The required mass flow of air, $\dot{m}_{air}$, can be obtained with the thermal balance in the ACC:

$$\dot{m}_{air} = \frac{\dot{Q}_{cond}}{c_{p,air} \cdot \Delta T_{air}} \qquad (2)$$

Where $\dot{Q}_{cond}$ is the thermal power to be exhausted through the condenser, from eq. (1), and $c_{p,air}$ the specific heat of the ambient air.

The parasitic consumption of the ACC fans is given by:

$$\dot{W}_{fan,ACC} = \frac{\dot{m}_{air} \cdot \Delta p_{air}}{\rho_{air} \cdot \eta_{fan}} \qquad (3)$$

Where Δp_{air} is the air static pressure drop to be overcome, ρ_{air} the air density and η_{fan} accounts for an overall fan efficiency value, including static, electromechanical and gear-box efficiencies and neglecting velocity pressure.

Assuming that the rest of variables remain unchanged for a specific thermal power, the parasitic consumption of the fans will only depend on the temperature rise of the air in the ACC, ΔT_{air}. If the outlet turbine pressure is allowed to be a variable value, then the saturation temperature in the condenser, T_{cond}, can be established according to the ambient temperature, in such a way that the temperature difference ΔT_{air} remains approximately constant. According to the scheme of Figure 6(b):

$$T_{cond} = T_{amb} + \Delta T_{ITD} = T_{amb} + \Delta T_{air} + \Delta T_{hot} \qquad (4)$$

The temperature difference at the hot side of the ACC, ΔT_{hot}, at design conditions is equal to the terminal temperature difference (*TTD*), a design parameter of the device (i.e., the design temperature difference

between inlet steam and outlet air) which is assumed to be 3 K in the simulation model. At part-load conditions, on the other hand, it is calculated by means of the NTU (Number of Transfer Units) method [38] according to the mass flow of steam. As a result, ΔT_{hot} may range from nearly 0 (at the lowest flow) to the *TTD* (at nominal steam flow). On the other hand, the saturation temperature, T_{cond}, can be regulated according to the ambient temperature to provide an almost constant temperature rise in the ACC, and therefore an approximately constant fan power consumption. In this way, the resulting value of air temperature difference, which determines the ACC fan parasitic consumption, can be estimated from the design parameter ΔT_{ITD} with the following expression:

$$\Delta T_{air} = \Delta T_{ITD} - \Delta T_{hot} \cong \Delta T_{ITD} - 3\ \mathrm{K} \qquad (5)$$

A typical value for the initial temperature difference of an ACC may be 16 K [41], and so it has been assumed in the simulation model. This leads to 13 K of air temperature difference.

3.4. Hybrid dry cooling system (Hy-DC)

The hybrid cooling system considered in the simulation model comprises two individual components: one for an ACC like the above described in section 3.3 and another for the LHS. Figure 7 shows the extended TRNSYS macro-component 'Cooling System' specified in Figure 5.

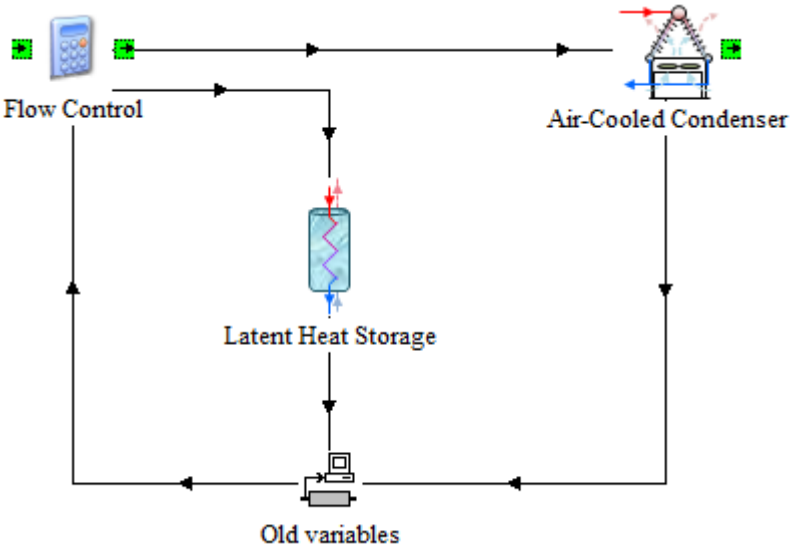

Figure 7: Screenshot of the TRNSYS macro-component for the cooling system

In addition, the subsystem model shown in Figure 7 includes a component that retains values from the previous time step ('Old variables') and an equation editor ('Flow Control') that handles the flow regulation of charge and discharge processes, explained in section 2.1.

The model of LHS is based on a simplified storage tank filled with a PCM that interchanges thermal energy with a water/steam flow. The water/steam flow may yield energy to the PCM (in a charge process), causing steam condensation when the fluid is at saturation conditions, or retrieve energy from the PCM (in a discharge process), producing water evaporation when saturation conditions are attained. The exchanged thermal power is calculated by a simplified heat balance:

$$\dot{Q} = U \cdot A \cdot \Delta T_{water-PCM} \qquad (6)$$

Where *U* is the overall heat transfer coefficient, *A* the heat exchange area and $\Delta T_{water-PCM}$ the temperature difference between the water/steam and the PCM. The same properties are considered for the whole PCM mass and heat losses are neglected. This implies a thermal efficiency of 100%, defined as the total energy obtained in a discharging process divided by the energy stored in the corresponding charging process. This assumption is based on a good insulation of the storage tank and considering that working temperatures in the LHS system are close to ambient temperatures. The maximum storage capacity is equal to the melting enthalpy of the PCM mass, so that only latent heat is considered. The storage level is calculated as the ratio of thermal energy stored in the PCM to the maximum storage capacity.

Table 4 summarizes the main parameters used in the simulation model of the ACC and LHS. The values concerning the ACC have been taken from several sources [41][42], whereas the useful PCM mass and operating hours of the storage system have been defined according to the assumptions stated in section 2.1. As seen in Table 4, a different amount of material is required for each PCM due to the different phase change enthalpies involved. Looking for the most advantageous conditions, the overall heat transfer coefficients for either charge or discharge processes are quite optimistic. Nevertheless, they are in accordance with the investigation by Merlin et al. [43], with a device based on a paraffin PCM-graphite composite material. Therefore, a heat enhancement mechanism is required to attain such heat transfer coefficients. Anyway, since the model follows a theoretical approach, the specific configuration of the heat enhancement device is not established and any other technique (finned tubes, PCM encapsulation …) that provides similar *U* values can also be considered.

Table 4: Main parameters considered in the simulation model of the ACC and LHS

Parameter	**Value**
Air-Cooled Condenser (ACC)	
Initial Temperature Difference (K)	16
Terminal Temperature Difference (K)	3
Fan Static Pressure (Pa)	120
Overall Fan Efficiency (%)	50
Latent Heat Storage (LHS)	
Overall Heat Transfer Coefficient during charge (W/m^2-K)	2000
Overall Heat Transfer Coefficient during discharge (W/m^2-K)	3000
Heat Exchange Area (m^2)	14000
Thermal energy stored (kJ)	$902 \cdot 10^6$
Useful mass required of PCM (t)	
RT35HC	3758
Paraffin C21	5673
Equivalent hours of operation (h)	3
Thermal Efficiency (%)	100

3.5. Operation strategies of the Hy-DC system

The gain in net electric power when using LHS for releasing the power block exhaust heat (LHS charging) can be described with the following expression:

$$\dot{W}_{gain\,(\mathrm{charge})} = \dot{W}_{gross,LHS} - \dot{W}_{gross,ACC} + \dot{W}_{fan,ACC\,(\mathrm{day})} \qquad (7)$$

Where $\dot{W}_{gross,LHS}$ is the gross electric power obtained when using LHS instead of the ACC during day time. It

is supposed to be higher or equal to the gross electric power when using the ACC for the same ambient conditions, $\dot{W}_{gross,ACC}$. $\dot{W}_{fan,ACC\,(day)}$ is the hypothetical parasitic consumption of the ACC at the same hour of the day without LHS charge. In this way, Figure 8 depicts a typical curve of $\dot{W}_{gain\,(charge)}$ as function of ambient temperature, obtained with the model of STE plant with RT35HC as PCM for nominal conditions of thermal power feeding the power block (see Table 1) and using the data included in Table 4.

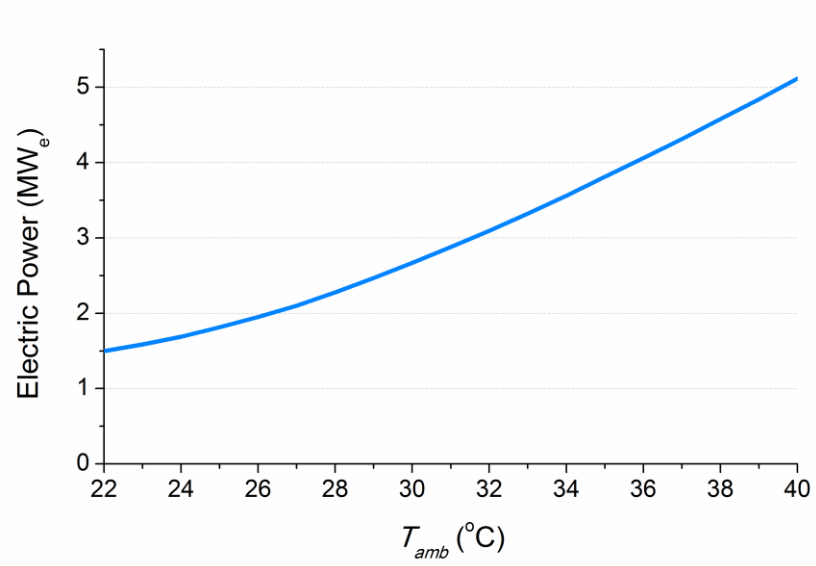

Figure 8: Estimated gain in net electric power as function of ambient temperature during a LHS charging process, with respect to ACC-only operation

During the night-time, when the power block stops, the exhaust heat stored in the LHS must be released to the environment, preferable during the coldest hours. This process (discharge of LHS) implies electric losses due to ACC fans consumption. Therefore, and as seen before, the higher the ambient temperature, the lower the air temperature difference ΔT_{air} and the higher the required air mass flow rates and parasitic consumptions $\dot{W}_{fan\,(discharge)}$. A typical curve for $\dot{W}_{fan\,(discharge)}$, obtained with eqs. (2) and (3) for a nominal mass flow rate of steam (see Table 1) and using the ACC data included in Table 4, is represented in Figure 9 as function of ambient temperature.

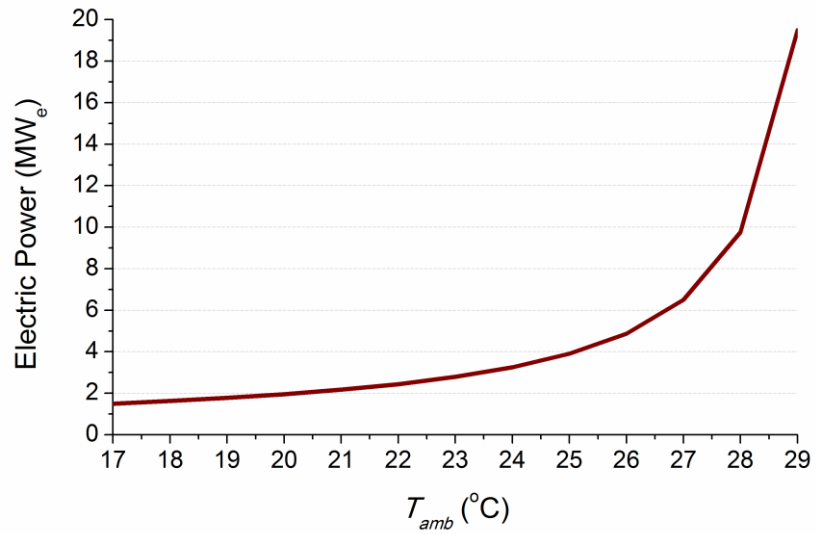

Figure 9: Fan parasitic consumptions of an ACC during a LHS discharging process as function of ambient temperature

Having a Hy-DC system will make sense only if the gain in net electric power during the daytime is higher than the ACC fan power consumed during the nighttime, i.e.:

$$\dot{W}_{gain\,(\mathrm{charge})} > \dot{W}_{fan\,(\mathrm{discharge})} \qquad (8)$$

If both curves are put together Figure 10 is obtained. Here a temperature difference between day and night of 10 K has been considered since it is a conservative value inferred from a preliminary study [45] carried out for several desert locations.

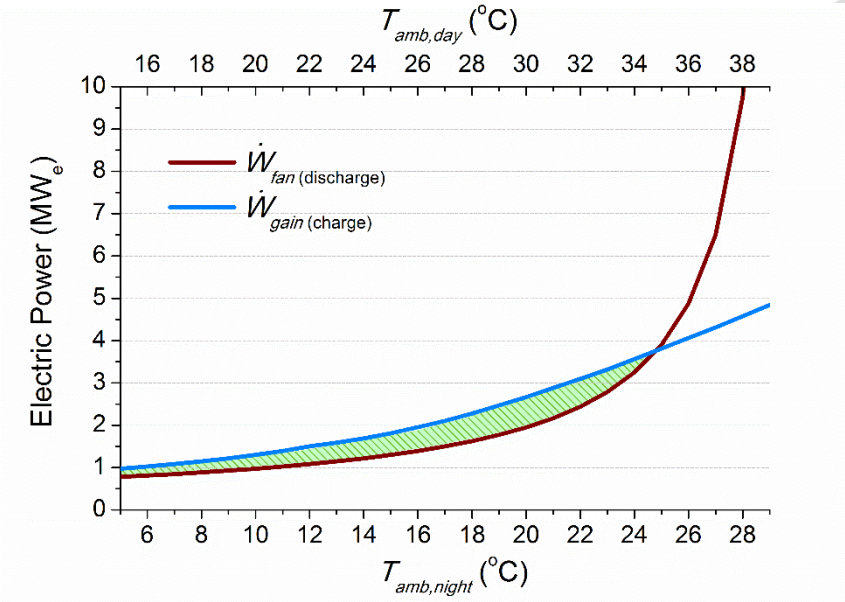

Figure 10: Estimated gain in net electric power for a LHS charging process and fan parasitic consumptions for a LHS discharging process as function of day and night ambient temperatures, considering 10 K of average difference between them

The difference between $\dot{W}_{gain\,(charge)}$ (blue line) and $\dot{W}_{fan\,(discharge)}$ (red line) curves represents the potential increase in net electricity at each moment by using the Hy-DC system in comparison with the Conv-DC system. If night ambient temperature is above 25 ºC, the parasitic losses due to the LHS discharge are higher than the hypothetical gains achieved by addressing the power block exhaust heat to the LHS during the daytime. Hence, the LHS discharge at night is not recommended when the ambient temperature at night is 25 ºC or higher. As shown in Figure 10, highlighted with a striped green pattern, the space between lines is not very large and therefore the expected overall gain in net production is not really high. Nevertheless, certain situations can make this balance more beneficial: if for example day-night ambient temperature differences are higher than 10 K, which depends on the specific temperature profile of the desert location, the red curve ($\dot{W}_{fan\,(discharge)}$) is shifted to the right and hence the condition imposed by eq. (8) will be more easily accomplished.

Another way to move the red curve ($\dot{W}_{fan\,(discharge)}$) to the right in Figure 10 is to implement a PCM in the LHS module with higher melting temperature, like Paraffin C21. This solution will allow higher condensing temperatures at night, increasing ΔT_{air} during discharge and therefore, according to eqs. (2) and (3), reducing fan parasitic consumptions. Even though power gain during daytime will also be reduced, lowering the blue line ($\dot{W}_{gain\,(charge)}$), the overall balance may be advantageous due to the specific shape of each curve. In this

way, the comparison between the simulation results obtained with both PCMs (RT35HC and Paraffin C21) for different locations will enable a preliminary assessment of this effect.

In the simulation model, the threshold value of ambient temperature for both charge and discharge of the LHS system is established at $T_{amb,ref} = T_{melt,PCM} - \Delta T_{air}$ (13 K less than the PCM melting temperature). This means that at night, LHS discharge process starts only when ambient temperature is below $T_{amb,ref}$. On the other hand, during the day time, the turbine exhaust heat is driven to the LHS to charge it, provided that the LHS is not full and the ambient temperature is above $T_{amb,ref}$. Otherwise, the outlet steam from the turbine is condensed at the ACC. Besides, the saturation temperature in the condenser, T_{cond}, during LHS charging processes is calculated by adding ΔT_{hot} to the PCM melting temperature ($T_{cond} = T_{melt,PCM} + \Delta T_{hot}$, which corresponds to $T_{melt,PCM} + 3\ K$ according to Table 4).

A further possibility for the Hy-DC system operation during daytime consists of sharing the heat rejection between the LHS and the ACC at the same time. Nevertheless, under such strategy the saturation pressure in the condenser must be carefully adjusted to allow the exhaust steam to be condensed by the ACC without jeopardizing the efficiency of the power block.

In the simulation model this exhaust heat sharing strategy is considered (labeled as Hy-DC_{sh}) and implemented by a linear function of ambient temperature. The fraction of exhaust steam mass flow rate driven to the LHS is obtained as $F_{LHS-ACC} = (T_{amb} - T_{amb,ref})/3$ and truncated to a value between 0 and 1. The same threshold and condensing temperatures as in the non-flow-sharing strategy are applied. This choice implies $T_{cond} = T_{melt,PCM} + 3\ \mathrm{K}$, explaining the denominator, equal to the *TTD*, in the expression for $F_{LHS-ACC}$ to provide the required slope of the linear function, Since ΔT_{hot} may range from 0 to 3 K depending on the steam flow (see section 3.3), the ACC will only be able to condense the exhaust steam at this specific T_{cond} when $T_{amb} \leq T_{amb,ref} + 3$. Above this ambient temperature, $F_{LHS-ACC} = 1$ and the whole exhaust steam flow is sent to the LHS. On the other hand, when the ambient temperature is below $T_{amb,ref}$, $F_{LHS-ACC} = 0$ and the entire flow of exhaust steam is led to the ACC. As a consequence, the LHS charging process is stopped. This approach attempts to maximize the gross efficiency of the power block by using the minimum value of saturation temperature required for LHS charging, without expecting an excessive increase in ACC fan consumptions.

3.6. Electric losses

Electric losses are estimated by Eq. (9):

$$\dot{W}_{loss}(\mathrm{kW}) = \dot{W}_{pump} + \dot{W}_{fan,ACC} + 750 + 120 \cdot F_{oper,SF} + 600 \cdot \max(F_{oper,SF}, F_{oper,PB}) + 150 \cdot \left(\dot{W}_{gross}/\dot{W}_{max}\right)^2 + 100 \cdot \left(\dot{Q}_{u,SF}/\dot{Q}_{max,SF}\right)^2 \quad (9)$$

Where $\dot{W}_{pump}$ includes pumping consumptions in the solar field, the thermal storage system and the power block. The parasitic consumption of ACC fans, $\dot{W}_{fan,ACC}$, is given by equation (3). The rest of the terms in eq. (9) are in line with the experience [21][22] in commercial STE plants and depend on the electric load ($\dot{W}_{gross}/\dot{W}_{max}$), the thermal load in the solar field ($\dot{Q}_{u,SF}/\dot{Q}_{max,SF}$) and whether the solar field or the power block is in operation. Factors $F_{oper,SF}$ and $F_{oper,PB}$ take the value 1 when the solar field or the power block are operated, respectively, or 0 otherwise.

3.7. Model's validation

Even though the whole model's validation can be found in previous works [21][22][33], this section shows the validity of the model by simulating a commercial STE plant in Spain with thermal storage and a wet cooling system, with similar features as those included in Table 1, for a typical sunny day (the 8th of March). Figure 11 represents gross and net electric power and electric losses, both from experimental real data (solid lines) and obtained from the plant simulation (dashed lines), with a time step of 5 min. DNI is also included in dotted blue line.

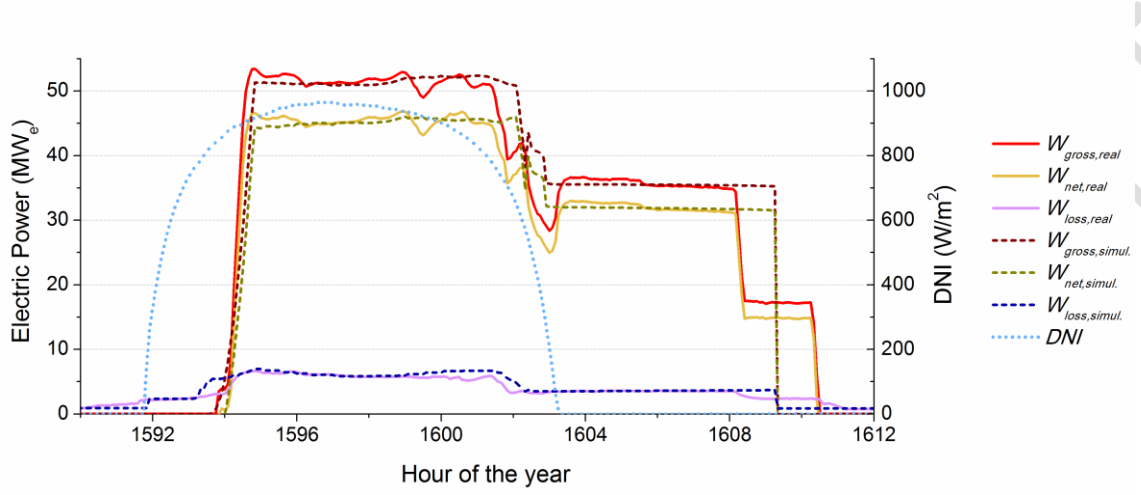

Figure 11: Comparison between real data from a commercial STE plant and the simulation results for a typical sunny day (8th of March)

As seen in Figure 11, a good agreement is observed between the real data and the simulation results. Considering a 24 h period, the root mean squared error is 5.9 MW_e for the gross electric power, 5.5 MW_e for the net electric power and 0.75 MW_e for the electric losses. This leads to differences of 0.66% in gross electricity and 0.48% in net electricity for the whole analysed day. These figures can be considered accurate enough for the purpose of this study.

4. Results and Discussion

Simulations with the already defined STE plant model at different locations are carried out throughout 1 year with a time step of 15 min, using different cooling approaches. Since the time step of available meteorological data is 1 h, DNI and ambient temperature data are interpolated to determine intermediate values in each simulation step.

Simulation results include the most relevant plant variables such as temperatures, thermal and electric power. Those values enable to obtain annual values of both gross and net electricity production and electric losses.

Firstly, an example of daily operation for a specific case is represented graphically to briefly understand the behaviour of the Hy-DC system approach. Then annual results for STE plants in different locations and using different operation strategies are shown. Comparison of the results using either Conv-DC or Hy-DC systems is made, allowing the inference of overall trends and recommendations. Finally, the results of the most promising options are used to perform a preliminary economic evaluation of the feasibility of the Hy-DC system as cooling concept.

4.1. Example of whole-day operation of the Hy-DC system

In order to explain the behaviour and benefits of a Hy-DC system, a specific example of step-by-step simulation is analysed for a representative day. The PCM chosen in this example for the LHS module is RT35HC. For simplicity, the operation strategy for LHS charging does not consider sharing heat rejection, so that the total steam flow to be condensed is driven to the LHS system. Since the parameters implemented in the model (see Table 4) involve 3 h of operation for the LHS, the charging process is scheduled 1 h after the solar noon, from 13 h to 16 h in solar time. This charging window has been chosen as an annual average of the hottest 3 hours of the day for all the locations considered, according to a preliminary analysis [45] of weather data. On the other hand, its discharge process is programmed to occur at the end of the night in order to take advantage of the coldest temperatures. This time schedule will be applied to every simulation performed in this work.

Figure 12 depicts the simulation results of the STE plant for a typical sunny summer day at the PSA (Almería, Spain), the 25th of June.

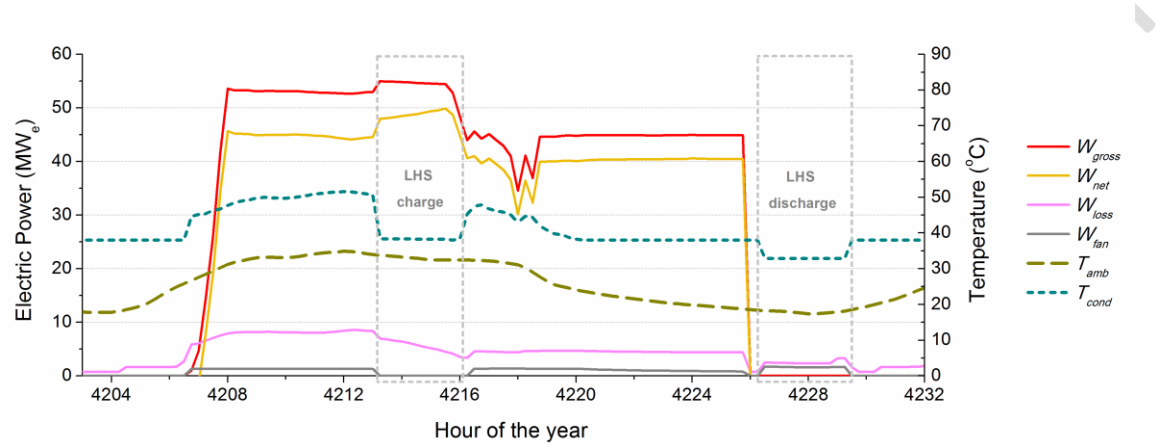

Figure 12: Simulation results for the STE plant with a Hy-DC system for a summer day at the PSA (Almería), including gross and net electric power, total electric losses, ACC fans parasitic consumptions, ambient and condenser temperatures

As seen in Figure 12, the condenser temperature at around hour 4214 decreases to its minimum value, 38 ºC, corresponding to the LHS charging process. Hence, the efficiency of the power block is improved and the gross electric power is increased comparing with hour 4212, for instance. In addition, since ambient temperature value remains above 22 ºC, the ACC is not used to condense the turbine outlet steam during such a process, leading to null consumption of the ACC fans. As a result of both effects, a significant increase in net electric power is observed during the LHS charging process (hours 4213 to 4216) with respect to the values obtained with the ACC operation (hour 4211, for example).

Figure 12 shows that the LHS charging period for this example day is not optimum because the maximum ambient temperature is given around hour 4212. Nevertheless, the optimum charging window is difficult to predict. Anyway, the differences in net production between an optimum charging strategy and the one applied in the simulation model would be relatively low. The maximum gain in electric power would be similar, for instance, to the difference in W_{gross} (red line) between hours 4210 and 4212, less than 0.5 MW. In the worst case, this value leads to an increase of 0.2% in the gross electricity production for this specific day by using an optimum LHS charging window, with respect to the production obtained from Figure 12. However, this estimation cannot be extrapolated to annual results since, according to the weather data, maximum ambient temperatures are commonly found during the chosen window.

4.2. Annual simulation results

Annual simulations have been performed for the locations and meteorological data described in section 2.2. Plant configurations include two versions of the cooling system: Conv-DC and Hy-DC. In the second case, two different strategies for charging the LHS have been implemented: circulating all the mass flow rate of steam from the turbine outlet through the LHS (Hy-$DC_{no\text{-}sh}$) or sharing the steam flow between ACC and LHS according to the ambient temperature (Hy-DC_{sh}), as explained in section 3.5. Two different PCMs (RT35HC and Paraffin C21) have been considered for filling the LHS module. In summary, five different cases have been simulated for each location. The complete table of results obtained from the STE plant simulation model can be found in Appendix B.

Firstly, annual electricity results of a STE plant with a Conv-DC system, which is taken as reference, are depicted in Figure 13. Net electricity production, parasitic consumptions of ACC fans and the rest of electric losses are represented as stacked columns, together with cumulative DNI values per year. The total height of each column stands for the gross annual electricity production, obtained as the sum of these three results.

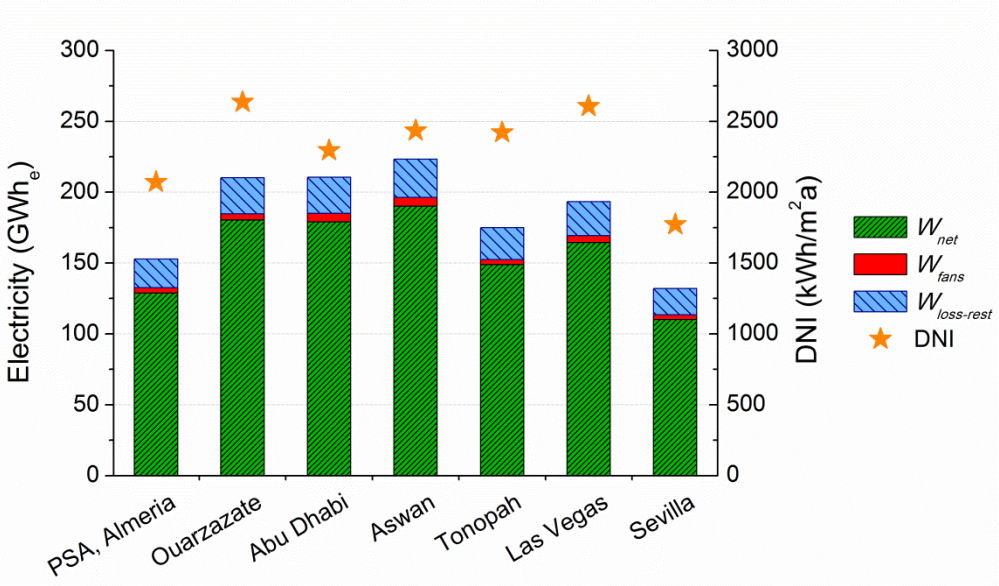

Figure 13: Annual electricity results of a STE plant with a Conv-DC system, including net electricity production, parasitic consumptions of ACC fans and the rest of electric losses for each location, together with annual DNI

The effect of latitude implies that the highest gross electricity yields are not those of the highest annual DNI, since the higher the latitude, the higher the optical losses in the solar field. Besides, annual ACC consumptions are observed to represent around 2-3% of gross electricity production.

The advantages of using a Hy-DC system can be evaluated through two terms: the increase in performance of the power block due to lower condensing pressure and the reduction of parasitic losses in ACC fans. The first of these terms can be associated with the expected gain in gross electricity production of STE plants with the Hy-DC concepts compared to the reference STE plant with a Conv-DC system (Figure 13). The resulting differences in gross annual electricity gain for each location and configuration are displayed in Figure 14.

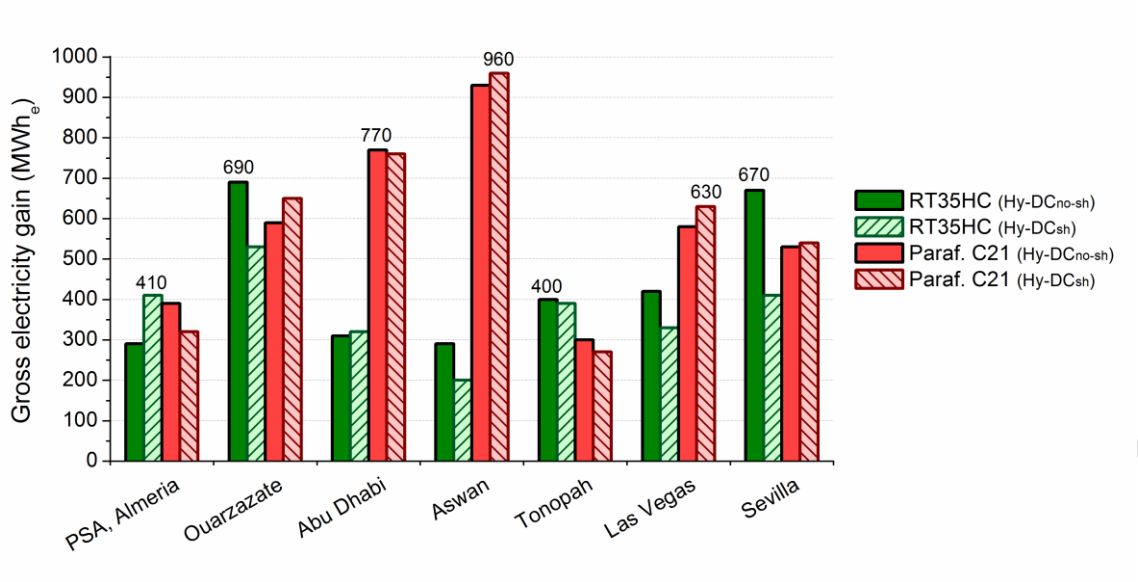

Figure 14: Expected gain in gross annual electricity of STE plants with Hy-DC systems with respect to the same plant with a Conv-DC system for each location, PCM and charging strategy

Figure 14 includes results for the two PCMs (RT35HC and Paraffin C21) and the two charging strategies considered for the LHS (Hy-DC$_{sh}$ and Hy-DC$_{no-sh}$). Even though in most cases the differences between both PCMs are not very important, in Abu Dhabi and Aswan the gains with Paraffin C21 are clearly higher than those with RT35HC. This effect seems to be related to the LHS regeneration at night. When ambient temperatures during the night-time are above the threshold value ($T_{amb,ref}$) established in section 3.5, 22 ºC for RT35HC, the LHS cannot be discharged and therefore it will not be available for the subsequent daily charging cycle. Since Abu Dhabi and Aswan show the highest values of minimum ambient temperature (see Table 3), the use of Paraffin C21 provides a more suitable threshold, 27 ºC, for LHS regeneration at night-time. On the other hand, ambient temperatures during the daytime determine the efficiency of the power block and hence the expected gain in annual production, according to Figure 8, provided that the LHS is available. Besides, the benefits obtained by sharing the heat rejection in LHS discharging processes (Hy-DC$_{sh}$) with respect to a non-flow-sharing strategy (Hy-DC$_{no-sh}$) are only observed for certain cases (PSA with RT35HC; Ouarzazate, Aswan and Las Vegas with Paraffin C21) and they do not represent a great amount of energy.

The expected savings in parasitic losses of ACC fans with respect to the Conv-DC system, which can be directly related to an increase in net electricity production, are depicted in Figure 15.

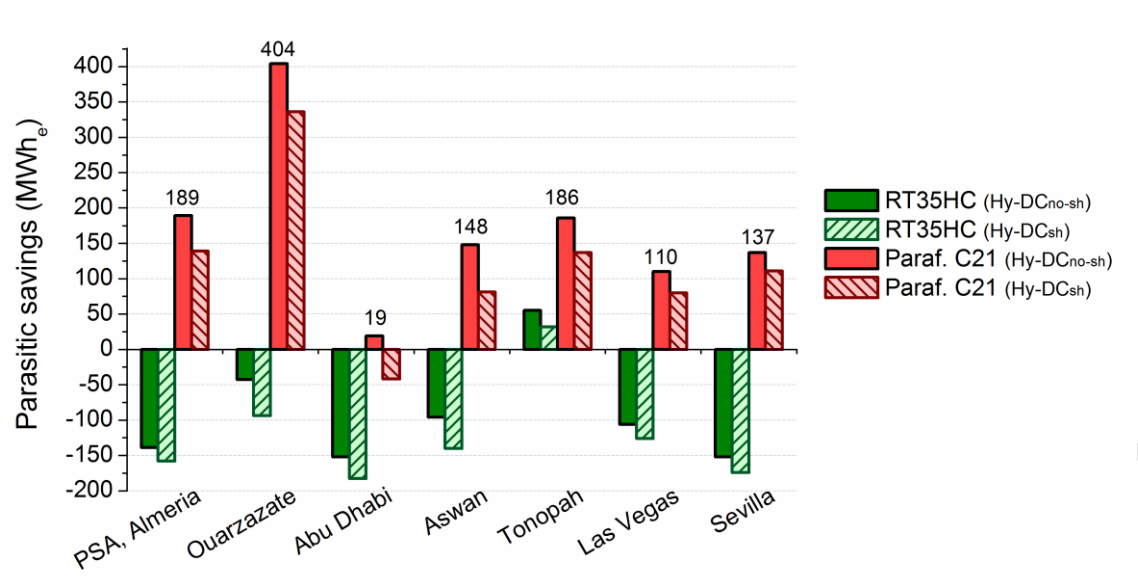

Figure 15: Expected savings in annual parasitic consumptions of ACC fans of STE plants with Hy-DC systems with respect to the same plant with a Conv-DC s system for each location, PCM and charging strategy

Figure 15 shows that, in almost every location, savings are only expected for Paraffin C21. RT35HC does not provide positive results in terms of ACC consumptions except for Tonopah, which presents the lowest ambient temperatures of all locations (see Table 3). This seems to reflect that melting temperature of RT35HC, 35 ºC, is too low for allowing a reduction in annual parasitic consumptions with respect to the Conv-DC system. That is, the low resulting values of ΔT_{air} during the night-time lead to great ACC consumptions for LHS discharging. These consumptions, integrated over the whole year, become higher than the expected savings by avoiding ACC operation at daytime. In this case, Hy-DC$_{sh}$ strategy gives always worse results than Hy-DC$_{no\text{-}sh}$ strategy.

The combined effect of both benefits (increase of cycle efficiency and savings in ACC consumptions) can be observed by means of net electricity production results. Relative differences in terms of percentage of net annual production are depicted in Figure 16 for each location, PCM (RT35HC or Paraffin C21) and operation strategy (non-shared or shared flow).

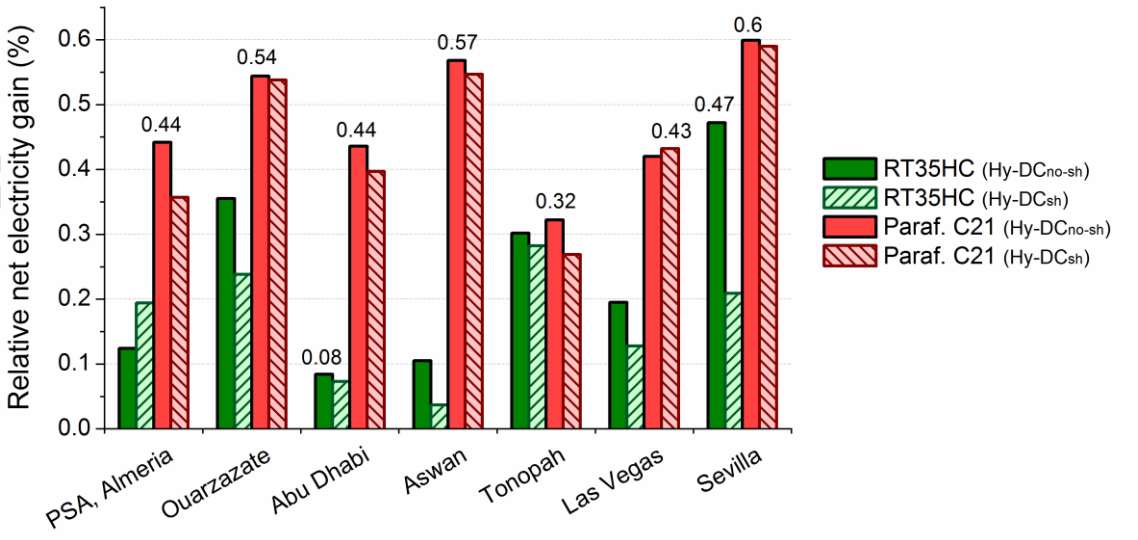

Figure 16: Relative gain in net annual electricity production for the direct LHS system with an Air-Cooled Condenser with respect to a dry-cooling system for different PCMs, locations and operation strategies

The maximum increase in relative net electricity production, 0.6%, is obtained for Sevilla for Paraffin C21 and the Hy-$DC_{no\text{-}sh}$ operation strategy. Relative gains shown in Figure 16 range between 0.32% and 0.6% for Paraffin C21 or between 0.08% and 0.47% for RT35HC in the case of non-flow-sharing strategy (Hy-$DC_{no\text{-}sh}$). On the other hand, sharing heat rejection (Hy-DC_{sh}) causes worse results in almost every case.

In general terms, the use of PCMs with higher melting points (Paraffin C21 in this case, compared with RT35HC) appears to provide better net annual production values according to Figure 16. Nevertheless, the convenience of a PCM with a higher or lower melting temperature seems to be related to the minimum ambient temperatures in the location under study (see Table 3). The differences between Paraffin C21 and RT35HC are higher in locations with higher minimum ambient temperatures (Abu Dhabi, Aswan), whereas the results are more similar for both PCMs in locations with lower minimum ones (Tonopah, Ouarzazate). The reasons are related to the high parasitic consumptions and the problems for regenerating the LHS during the night-time when RT35HC is considered. This effect suggests that the use of PCMs with higher melting temperatures may be advisable for locations for high expected ambient temperatures at night. Nevertheless, maximum temperatures are also relevant since they determine day-night temperature differences. As explained in section 3.5, the higher these differences, the higher the annual gains in net electricity production with the Hy-DC concept.

When comparing Hy-$DC_{no\text{-}sh}$ and Hy-DC_{sh} strategies either a decrease in performance or no major difference is observed for most locations. An exception to this behaviour is the PSA with RT35HC, suggesting that the sharing strategy could be advantageous for specific cases. Even though the annual performance does not seem to advise that option, maybe a more careful look should be taken to the monthly evolution of weather data at the specific location. The flow-sharing strategy may be recommended when the expected ambient temperatures are close to the threshold values ($T_{amb,ref}$) defined in section 3.5. In this way, the issues explained in that section regarding charging and discharging cycles and day-night differences in ambient temperature can be helpful.

4.3. Preliminary economic estimation and feasibility regarding PCM costs

A rough economic estimation has been performed taking into account the maximum gain in net electricity production from the annual results. This analysis aims to determine a range of PCM costs that would allow the concept to be feasible. Considering the annual simulation results included in Table B.1, the maximum gain in terms of net annual electricity production corresponds to a STE plant located in Aswan with a Hy-DC system with Paraffin C21 as PCM, i. e. 1080 MWh. Assuming average electricity prices of 150 €/MWh [11][44] and a plant lifetime of 25 years, the maximum expected income by using the LHS system will be:

$$Income = 1080\ \text{MWh/year} \cdot 150\ €/\text{MWh} \cdot 25\ \text{years} = 4.05 \cdot 10^6\ € \qquad (10)$$

In first approach (i. e. considering only the PCM and neglecting equipment and financing costs related to LHS), the implementation of a Hy-DC system will be cost-effective if PCM price fulfils the following ratio:

$$\frac{Cost_{PCM}\ (€/\text{kg})}{\Delta h\ (\text{kJ/kg})} < \frac{Income\ (€)}{Q_{LHS}\ (\text{kJ})} = \frac{4.05 \cdot 10^6\ €}{902\ \cdot\ 10^6\ \text{kJ}} = 4.5 \cdot 10^{-3}\ €/\text{kJ} \qquad (11)$$

Where $Q_{LHS} = 902 \cdot 10^6$ kJ is the total amount of thermal energy stored in the LHS (see Table 4) and Δh is the specific latent heat of the PCM. If we consider RT35HC, which has a latent heat of 240 kJ/kg [45] and an expected cost of 11 €/kg (according to a real offer given by the manufacturer [23]), the cost-to-latent heat ratio is $4.58 \cdot 10^{-2}$ €/kJ and hence far beyond the limit value given by eq. (11). Although paraffins have lower costs

[46], they do not seem to provide the required figures regarding cost-to-latent heat ratio either. Promising PCMs for this application could be hydrated salts, with costs around 0.3-0.5 €/kg and latent heat around 100-200 kJ/kg [45]. However, their expected issues [47] in terms of long-term stability and congruent melting/freezing should be further tested and confirmed.

It must be remarked that this analysis is just preliminary and assumes a high uncertainty. Trying to follow the most simplified approach, it is mainly focused on PCM costs, but device manufacturing, operation & maintenance, financing, etc. are not considered. Besides, the economic parameters applied are based on countries with strong incentives to STE plants [44] and their extrapolation to other environments should be carefully analysed.

5. Conclusions

In this work, a new concept of hybrid dry cooling (Hy-DC) system for STE plants in desert areas is analysed. Such cooling system consists of a combination of latent heat storage (LHS) containing a phase change material (PCM) connected in parallel with an air-cooled condenser (ACC). This concept takes advantage of the coldest ambient temperature at night to release the exhaust heat from the turbine, increasing power block efficiency and reducing parasitic consumptions.

A simulation model of a solar thermal electricity plant with this Hy-DC system is developed to compare its performance in terms of net production with a conventional dry cooling system based on ACC only. For this purpose, seven desert locations and two different PCMs (RT35HC, with a melting point of 35 ºC, and Paraffin C21, with 40.2 ºC) have been considered for the simulations, together with two different strategies for exhaust heat rejection during daytime.

The increase in net annual electricity production ranges from 0.3% to 0.6% for Paraffin C21 or from 0.1% to 0.5% for RT35HC. In addition, the differences between both PCMs are higher for locations with higher ambient temperatures during the night-time. In these locations, the high ACC consumptions and the difficulties for LHS regeneration due to the lower melting temperature puts RT35HC in a disadvantage against Paraffin C21. This suggests that the use of PCMs with higher melting points would be advisable for locations with high night-time ambient temperatures.

In general terms, the operation strategy that provides higher electricity outputs consists of condensing the whole exhaust steam flow by using the latent storage module when daily ambient temperatures are the highest.

From annual simulation results, a preliminary economic estimation based on the cost-to-latent heat ratio of the PCM to be implemented in the LHS has been performed for a STE plant with a Hy-DC system. Even for the case with maximum gain in terms of net annual electricity production, the cost-to-latent heat ratio of the PCM should be below $4.5 \cdot 10^{-3}$ €/kJ, using the data and conditions considered in this work, to make this concept feasible. However, the PCMs analysed in this study (RT35HC, Paraffin C21) present too high cost-to-latent heat ratios for the Hy-DC to be a really cost-effective solution for STE plant cooling.

In conclusion, investigation on low-cost PCMs with higher melting temperatures may be interesting to improve the performance of the proposed Hy-DC concept. Nevertheless, issues like electricity prices along the plant lifetime and both materials and equipment cost for the latent storage system should be considered for a proper assessment of its expected feasibility.

Appendix A: Summary of calculations applied in the simulation model.

The useful thermal power, $\dot{Q}_u$, gained by the working fluid in a PT collector is obtained with the following expression:

$$\dot{Q}_u = \eta_{opt,0^\circ}\, \eta_{clean}\, \eta_{sh}\, K(\theta)\, G_b \cos(\theta)\, A_c - \dot{Q}_{loss} \qquad (A.1)$$

Where G_b is the direct normal irradiance, A_c the net collector aperture area, θ the incidence angle, $K(\theta)$ the incidence angle modifier, $\eta_{opt,0^\circ}$ the peak optical efficiency, η_{clean} the cleanliness factor, η_{sh} the shadowing factor between adjacent collector rows and $\dot{Q}_{loss}$ the thermal losses to the environment. The incidence angle, θ, is directly obtained from the 'Radiation Processor' (*Type16g*), a standard component of the TRNSYS library.

The incidence angle modifier $K(\theta)$ is calculated with the following equation (with θ in °), taken from the experimental characterization of EuroTrough-II collectors [35]:

$$K(\theta) = 1 - (5.25 \cdot 10^{-4} \cdot \theta + 2.86 \cdot 10^{-5} \cdot \theta^2)/\cos\theta \qquad (A.2)$$

The thermal losses in the PT collectors, $\dot{Q}_{loss}$, are calculated with the equation below, evaluated from outdoor tests [36] at the PSA for standard SCHOTT PTR®70 receiver tubes:

$$\dot{Q}_{loss} = \left(0.342 \cdot \Delta T_{fluid-amb} + 1.163 \cdot 10^{-8} \cdot \Delta T_{fluid-amb}^4\right) \cdot L \qquad (A.3)$$

Where the result, $\dot{Q}_{loss}$, is given in W, $\Delta T_{fluid\text{-}amb}$ is the difference between the average temperature of the fluid and the ambient temperature, in K, and L is the length of the absorber pipe section to be considered, in m.

To reproduce a quasi-dynamic behaviour of the system in transient conditions, the model performs an energy balance taking into account the effect of thermal inertia due to the mass of fluid, m_{fluid}, and pipe, m_{pipe}, in a time step Δt. The useful energy absorbed by the fluid, $\dot{Q}_u \Delta t$, can be expressed as a sum of energy interchanged in each component. If the effect of kinetic energy due to the variation of fluid speed is neglected, the outlet temperature of the fluid at the collector's outlet, T_{out}, can be thus obtained knowing the rest of the elements in:

$$\dot{Q}_u \Delta t = m_{fluid}\, c_{p,fluid} \Delta \bar{T}_{fluid} + m_{pipe}\, c_{p,pipe} \Delta \bar{T}_{pipe} + \dot{m}\, c_{p,fluid} (T_{out} - T_{in}) \Delta t \qquad (A.4)$$

Where $\dot{m}$ is the mass flow rate, ΔT_{pipe} and ΔT_{fluid} the increase in the average temperature of the pipe and the fluid, respectively, since the previous time step, $c_{p,pipe}$ and $c_{p,fluid}$ the specific heat capacity of pipe and fluid and T_{in} the temperature of the fluid at the collector's inlet. Assuming that the average temperature increase is the same for the fluid (ΔT_{fluid}) and piping (ΔT_{pipe}), and it is equal to the average increase of inlet and outlet temperatures, $\Delta T_{fluid} = \Delta T_{pipe} = (\Delta T_{in} + \Delta T_{out})/2$, an explicit function for the outlet temperature can be obtained from Eq. (A.4), thus enabling a simplified approach.

The pressure loss due to friction through a straight section of pipe is calculated with the Darcy-Weisbach equation [37]:

$$\Delta p = {}^1/_2\, f \rho v^2 {}^L/_D \qquad (A.5)$$

In Eq. (A.5) the pressure loss Δp is a function of the 'length to diameter' ratio of the pipe, *L/D*, the fluid velocity, v, and density, ρ, and the Darcy friction factor, f, which is calculated with the Poiseulle's law [37] in case of laminar flow ($Re < 2100$) or with the Chen correlation [48] in case of turbulent flow ($Re > 2100$). The same equation (A.5) is used to calculate the pressure drop due to friction in accessories by applying an equivalent value of *L/D* ratio for each accessory (elbows, ball joints, etc.) [37].

From the calculated pressure loss Δp, the electric power required to pump a mass flow rate, $\dot{m}$, of fluid is obtained with:

$$\dot{W}_{pump} = \frac{\dot{m} \cdot \Delta p}{\rho \cdot \eta_{pump}} \qquad (A.6)$$

Where ρ is the fluid density and η_{pump} the overall efficiency of the pump.

The 2-tank storage system is modelled with two components (hot and cold) that reproduce the behaviour of variable volume tanks with molten salt as heat storage medium. For each tank, the following differential equation is evaluated at each time step:

$$\dot{Q}_{in} - \dot{Q}_{loss} = \frac{dQ}{dt} + \dot{Q}_{out} \qquad (A.7)$$

Eq. A.7 represents an energy balance between the useful inlet thermal power ($\dot{Q}_{in} = \dot{m}_{in} c_p T_{in}$), the outlet thermal power ($\dot{Q}_{out} = \dot{m}_{out} c_p T$), thermal losses to the environment ($\dot{Q}_{loss}$) and the variation of thermal energy of the fluid inside the tank ($Q = m c_p T$). The thermal losses are obtained with:

$$\dot{Q}_{loss} = U \cdot A \cdot (T - T_{amb}) \qquad (A.8)$$

Where U is the overall heat losses coefficient, A is the whole inner surface of the tank, T the current fluid temperature in the tank and T_{amb} the ambient temperature.

Heat exchangers are characterized with their UA product, i.e. the overall heat transfer coefficient times the exchange area. In the model, the ratio of UA to its nominal value UA_{ref} is estimated from the relative mass flow rate ($\dot{m}/\dot{m}_{ref}$) through the HX with the following expression [49]:

$$\frac{UA}{UA_{ref}} = \left(\frac{\dot{m}}{\dot{m}_{ref}}\right)^{0.8} \qquad (A.9)$$

The UA product enables the calculation of temperature differences in the HX at part-load conditions if we know the heat capacity rate ($C = \dot{m} c_p$) for each current ($C_1 \Delta T_1 = C_2 \Delta T_2 = \dot{Q}$). The exchanged heat, $\dot{Q}$, can be obtained with:

$$\dot{Q} = \varepsilon \, C_{min} \Delta T_{max} \qquad (A.10)$$

Where C_{min} is the minimum heat capacity rate of the two fluid streams ($C_{min} = min(C_1;C_2)$), ΔT_{max} is the maximum possible temperature difference in the HX (i.e. the absolute difference between the two inlet temperatures) and ε is the effectiveness.

For HXs in counter-current flow, with no phase change (HX of the 2-tank storage; preheater, reheater and superheater of the steam generator), the effectiveness is calculated [38] with:

$$\varepsilon = \frac{1 - exp(-NTU \cdot (1 + C_r))}{1 - C_r \cdot exp(-NTU \cdot (1 + C_r))} \qquad (A.11)$$

Where C_r is the heat capacity ratio ($C_r = C_{min} / C_{max}$) and NTU is the Number of Transfer Units ($NTU = UA / C_{min}$).

For counter-current flow HXs in which a phase change occurs (feedwater heaters and deaerator of the PB; evaporator of the steam generator), $C_r = 0$. In this case the effectiveness is obtained [38] with:

$$\varepsilon = 1 - exp(-NTU) \qquad (A.12)$$

The UA product for a counter-current flow HX at design conditions (UA_{ref}) can be determined from the exchanged heat, $\dot{Q}_{ref}$, and the corresponding temperature differences at each side, hot and cold, of the HX

(ΔT_{hot} and ΔT_{cold}) by means of the *LMTD* (logarithmic mean temperature difference [38]):

$$\dot{Q}_{ref} = UA_{ref} \cdot LMTD = UA_{ref} \frac{\Delta T_{hot} - \Delta T_{cold}}{ln(\Delta T_{hot}/\Delta T_{cold})} \quad (A.13)$$

The power block has been modelled by evaluating the pressure, enthalpy and mass flow rate of the fluid at each point of the circuit. Heat transfer coefficients and temperature differences in the feedwater heaters and the deaerator are calculated with the above-described method for HXs. The Spencer-Cotton-Cannon method [39] is applied to calculate both the isentropic efficiency of the turbine and the electro-mechanical efficiency of the electric generator.

The calculation of pressure values at each stage of the turbine is based on the Stodola law [50], assuming equal-enthalpy steps in the extraction pressures for a whole turbine body (either high or low pressure). An iterative process is then carried out to determine the mass flow through each turbine extraction. The enthalpy balance at each point of the turbine is calculated with:

$$h_{in} - h_{out} = \eta_{s,turb} \cdot (h_{in} - h_{out,s}) \quad (A.14)$$

Where h_{in} and h_{out} are the actual enthalpy values at the inlet and outlet of the turbine stage, $h_{out,s}$ is the outlet enthalpy corresponding to an isentropic expansion of the steam and $\eta_{s,turb}$ is the isentropic efficiency.

Once the mass flow proportion in each turbine extraction (F_{ext}) and the enthalpies at each point of the circuit are known, the specific work (in J/kg) for a specific turbine stage (i) can be calculated from the enthalpy difference, Δh_i (also in J/kg), between the inlet and outlet, the sum of previous extractions and the electro-mechanical efficiencies of the turbine ($\eta_{m,turb}$) and the generator (η_{gener}):

$$w_i = \eta_{m,turb} \cdot \eta_{gener} \cdot \Delta h_i \cdot \left(1 - \sum_1^{i-1} F_{ext}\right) \quad (A.15)$$

Finally, the gross electric power, in W, is calculated with the inlet mass flow rate of steam ($\dot{m}_{in,turb}$, in kg/s) to the turbine and the sum of specific works (in J/kg) in each turbine stage:

$$\dot{W}_{gross} = \dot{m}_{in,turb} \sum w_i \quad (A.16)$$

The main additional parameters assumed in the simulation model of the STE plant are summarized in Table A.1.

Table A.1: Main additional parameters assumed in the simulation model of the STE plant

Parameter	Value
Equivalent *L/D* for elbows and ball joints	37.5
Equivalent *UA* value for molten salt tanks (W/K)	28
Nominal Δ*T* in hot / cold side of HX in the 2-tank storage system (K)	5 / 6
Nominal Δ*T* in hot / cold side of feedwater heaters in PB (K)	1.7 / 5
Nominal Δ*T* in hot / cold side of steam generator (K)	11 / 30
Nominal efficiency of thermal oil pumps (%)	85
Nominal efficiency of molten salt pumps (%)	76
Nominal efficiency of water pumps in PB (%)	74
Nominal steam inlet pressure to the turbine (Pa)	$10.5 \cdot 10^6$
Nominal isentropic efficiency of high / low pressure turbine (%)	85.5 / 89.5
Nominal electro-mechanical efficiency of the turbine (%)	99.5

Nominal electro-mechanical efficiency of the electric generator (%)	98.5

Appendix B. Annual results of electricity production

Table B.1 summarizes the annual results of gross and net production obtained from the simulation model for each plant configuration, PCM and location, including also the annual parasitic energy consumed by the ACC fans. The increase in net electricity production obtained with the hybrid version compared to the dry-cooling option is specified as additional columns in both absolute and relative terms.

Table B.1: Annual results of electricity production using different cooling system configurations, PCMs and locations

Location	Configuration	PCM	W_{gross}	W_{fans}	W_{net}	ΔW_{net} (LHS)	
			(GWh_e)	(GWh_e)	(GWh_e)	(MWh_e)	(%)
PSA, Almería, Spain	Conv-DC	-	152.74	3.688	128.89		
PSA, Almería, Spain	Hy-DC_{no-sh}	RT35HC	153.03	3.827	129.05	160	0.12
PSA, Almería, Spain	Hy-DC_{sh}	RT35HC	153.15	3.846	129.14	250	0.19
PSA, Almería, Spain	Hy-DC_{no-sh}	Paraf. C21	153.13	3.499	129.46	570	0.44
PSA, Almería, Spain	Hy-DC_{sh}	Paraf. C21	153.06	3.549	129.35	460	0.36
Ouarzazate, Morocco	Conv-DC	-	210.16	4.384	180.3		
Ouarzazate, Morocco	Hy-DC_{no-sh}	RT35HC	210.85	4.427	180.94	640	0.35
Ouarzazate, Morocco	Hy-DC_{sh}	RT35HC	210.69	4.478	180.73	430	0.24
Ouarzazate, Morocco	Hy-DC_{no-sh}	Paraf. C21	210.75	3.98	181.28	980	0.54
Ouarzazate, Morocco	Hy-DC_{sh}	Paraf. C21	210.81	4.048	181.27	970	0.54
Abu Dhabi, UAE	Conv-DC	-	210.54	5.98	179.0		
Abu Dhabi, UAE	Hy-DC_{no-sh}	RT35HC	210.85	6.132	179.15	150	0.08
Abu Dhabi, UAE	Hy-DC_{sh}	RT35HC	210.86	6.163	179.13	130	0.07
Abu Dhabi, UAE	Hy-DC_{no-sh}	Paraf. C21	211.31	5.961	179.78	780	0.44
Abu Dhabi, UAE	Hy-DC_{sh}	Paraf. C21	211.3	6.022	179.71	710	0.40
Aswan, Egypt	Conv-DC	-	223.37	6.211	190.1		
Aswan, Egypt	Hy-DC_{no-sh}	RT35HC	223.66	6.307	190.3	200	0.11
Aswan, Egypt	Hy-DC_{sh}	RT35HC	223.57	6.351	190.17	70	0.04
Aswan, Egypt	Hy-DC_{no-sh}	Paraf. C21	224.3	6.063	191.18	1080	0.57
Aswan, Egypt	Hy-DC_{sh}	Paraf. C21	224.33	6.13	191.14	1040	0.55
Tonopah, USA	Conv-DC	-	174.89	3.511	148.96		
Tonopah, USA	Hy-DC_{no-sh}	RT35HC	175.29	3.456	149.41	450	0.30
Tonopah, USA	Hy-DC_{sh}	RT35HC	175.28	3.479	149.38	420	0.28
Tonopah, USA	Hy-DC_{no-sh}	Paraf. C21	175.19	3.325	149.44	480	0.32
Tonopah, USA	Hy-DC_{sh}	Paraf. C21	175.16	3.374	149.36	400	0.27
Las Vegas, USA	Conv-DC	-	193.37	4.799	164.45		
Las Vegas, USA	Hy-DC_{no-sh}	RT35HC	193.79	4.905	164.77	320	0.19
Las Vegas, USA	Hy-DC_{sh}	RT35HC	193.7	4.925	164.66	210	0.13
Las Vegas, USA	Hy-DC_{no-sh}	Paraf. C21	193.95	4.689	165.14	690	0.42
Las Vegas, USA	Hy-DC_{sh}	Paraf. C21	194	4.719	165.16	710	0.43
Sevilla, Spain	Conv-DC	-	132	3.452	110.13		
Sevilla, Spain	Hy-DC_{no-sh}	RT35HC	132.67	3.604	110.65	520	0.47
Sevilla, Spain	Hy-DC_{sh}	RT35HC	132.41	3.626	110.36	230	0.21
Sevilla, Spain	Hy-DC_{no-sh}	Paraf. C21	132.53	3.315	110.79	660	0.60
Sevilla, Spain	Hy-DC_{sh}	Paraf. C21	132.54	3.341	110.78	650	0.59

References

[1] SolarPACES, CSP Projects around the world, SolarPACES-Solar Power and Chemical Energy Systems. IEA Technology Collaboration Programme. Available from: http://www.solarpaces.org/csp-technologies/csp-projects-around-the-world/, 2020 [accessed 2 January 2020].

[2] N. Bracken, J. Macknick, A. Tovar-Hastings, P. Komor, M. Gerritsen, S. Mehta. Concentrating Solar Power and Water Issues in the US Southwest. NREL Technical Report NREL/TP-6A50-61376, Contract No. DE-AC36-08GO28308. Joint Institute for Strategical Energy Analysis, USA. 2015.

[3] C.S. Turchi, M.J. Wagner, C.F. Kutscher. Water Use in Parabolic Trough Power Plants: Summary Results from WorleyParsons' Analyses. NREL Technical Report NREL/TP-5500-49468, Contract No. DE-AC36-08GO28308. National Renewable Energy Laboratory, USA. 2010.

[4] X. Xu, K. Vignarooban, B. Xu, K. Hsu, A.M. Kannan. Prospects and problems of concentrating solar power technologies for power generation in the desert regions. Renew Sustain Energy Rev 53 (2016) 1106-1131.

[5] A. Poullikkas, G. Kourtis, I. Hadjipaschalis. An overview of CSP cooling systems. In: I. Michaelides, E. Charalambides, editors. Proceedings of the 3rd International Conference on Renewable Energy Sources and Energy Efficiency. 19 – 20 May 2011, Nicosia, Cyprus. ISBN978-9963-567-02-7.

[6] A. Ashwood, D. Bharathan, Hybrid Cooling Systems for Low-Temperature Geothermal Power Production. Technical Report NREL/TP-5500-48765. National Renewable Energy Laboratory. Golden, CO, USA, 2011.

[7] H. Hu, Z. Li, Y. Jiang, X. Du. Thermodynamic characteristics of thermal power plant with hybrid (dry-wet) cooling system. Energy 147 (2018) 729-741.

[8] H. Wei, X. Huang, L. Chen, L. Yang, X. Du. Performance prediction and cost-effectiveness analysis of a novel natural draft hybrid cooling system for power plants. Appl Energy 262 (2020) 114555.

[9] C.R. Williams, M. Rasul. Feasibility of a hybrid cooling system in a thermal power plant. In: Proceedings of the 3rd IASME/WSEAS International Conference on Energy & Environment. 23 - 25 February 2008, Cambridge, UK.

[10] C. Richter. Hochtemperatur-Solarthermische Stromerzeugung: EFCOOL - wassereffiziente Kühlung solarthermischer Kraftwerke. BMU-Programm, Final Report. 2007. https://doi.org/10.2314/GBV:599084448

[11] L. Pistocchini, M. Motta. Feasibility Study of an Innovative Dry-Cooling System with Phase-Change Material Storage for Concentrated Solar Power Multi-MW Size Power Plant. J Sol Energy Eng 133 (2011) 031010-1-8.

[12] C. Pan, N. Vermaak, C. Romero, S. Neti, S. Hoenig, C-H. Chen, R. Bonner. Cost estimation and sensitivity analysis of a latent thermal energy storage system for supplementary cooling of air cooled condensers. Appl Energy 224 (2018) 52-68.

[13] F. Agyenim, P. Eames, M. Smyth. A comparison of heat transfer enhancement in a medium temperature thermal energy storage heat exchanger using fins. Sol Energy 83 (2009) 1509-1520.

[14] R. Bayón, E. Rojas, L. Valenzuela, E. Zarza, J. León. Analysis of the experimental behaviour of a 100 kWth latent heat storage system for direct steam generation in solar thermal power plants. Appl Therm Eng 30 (2010) 2643–2651.

[15] V. Palomba, V. Brancato, A. Frazzica. Experimental investigation of a latent heat storage for solar cooling applications. Appl Energy 199 (2017) 347-358.

[16] J.M. Marín, B. Zalba, L.F. Cabeza, H. Mehling. Improvement of a thermal energy storage using plates with paraffin-graphite composite. Int J Heat Mass Tran 48 (2005) 2561-2570.

[17] R. Al-Shannaq, M.M. Farid. A novel graphite-PCM composite sphere with enhanced thermo-physical properties. Appl Therm Eng 142 (2018) 401-409.
[18] A. Barba, M. Spiga. Discharge mode for encapsulated PCMs in storage tanks. Sol Energy 74 (2003) 141-148.
[19] E. Alehosseini, S.M. Jafari. Nanoencapsulation of phase change materials (PCMs) and their applications in various fields for energy storage and management. Adv Colloid Interface Sci (2020) 102226 (in press).
[20] Solar Millenium. The parabolic trough power plants Andasol 1 to 3. Solar Millenium AG. Available from: http://large.stanford.edu/publications/power/references/docs/Andasol1-3engl.pdf, 2008 [accessed 2 January 2020].
[21] M. Biencinto, R. Bayón, E. Rojas, L. González. Simulation and assessment of operation strategies for solar thermal power plants with a thermocline storage tank. Sol Energy 103 (2014) 456–472.
[22] M. Biencinto, L. González, L. Valenzuela, E. Zarza. A new concept of solar thermal power plants with large-aperture parabolic-trough collectors and sCO_2 as working fluid. Energy Convers Manage 199 (2019) 112030.
[23] Rubitherm. Available from: http://www.rubitherm.eu/, 2020 [accessed 2 January 2020].
[24] N. Ukrainczyk, S. Kurajica, J. Sipusic. Thermophysical Comparison of Five Commercial Paraffin Waxes as Latent Heat Storage Materials. Chem Biochem Eng 24(2) (2010) 129-137.
[25] R. Bayón, M. Biencinto, E. Rojas, N. Uranga. Study of Hybrid Dry Cooling Systems for STE Plants Based on Latent Storage. In: Proceedings of the ISEC 2018 International Sustainable Energy Conference, October 2018, Graz, Austria.
[26] NIST Webbook. Heneicosane, Phase Change Data. Available from: https://webbook.nist.gov/cgi/cbook.cgi?ID=C629947&Units=SI&Mask=4#Thermo-Phase, 2020 [accessed 2 January 2020].
[27] A. Abhat. Low temperature latent heat thermal energy storage: heat storage materials. Sol Energy 30 (4) (1983) 313-332.
[28] PSA. Plataforma Solar de Almería, Spain. Available from: http://www.psa.es/en/, 2019 [accessed 2 January 2020].
[29] MASEN. Moroccan Agency of Sustainable Energy. Available from: http://www.masen.ma/en/, 2019 [accessed 2 January 2020].
[30] SAM. System Advisor Model, Version 2017.9.5, Solar resource files. National Renewable Energy Laboratory, USA. Available from: https://sam.nrel.gov/, 2017 [accessed 3 October 2017].
[31] S.A. Klein et al. TRNSYS 17: A Transient System Simulation Program. Solar Energy Laboratory, University of Wisconsin, Madison, USA. Available from: http://sel.me.wisc.edu/trnsys, 2013 [accessed 19 December 2016].
[32] M. Biencinto, L. González, E. Zarza, L.E. Díez, J. Muñoz-Antón. Performance model and annual yield comparison of parabolic-trough solar thermal power plants with either nitrogen or synthetic oil as heat transfer fluid. Energy Convers Manage 87 (2014) 238–249.
[33] M. Biencinto, L. González, L. Valenzuela. A quasi-dinamic simulation model for direct steam generation in parabolic troughs using TRNSYS. Appl Energy 161 (2016) 133-142.
[34] M. Biencinto, M.J. Montes, L. Valenzuela, L. González. Simulation and comparison between fixed and sliding-pressure strategies in parabolic-trough solar power plants with direct steam generation. Appl Therm Eng 125 (2017) 735-745.
[35] M. Geyer, E. Lüpfert, R. Osuna, A. Esteban, W. Schiel, A. Schweitzer, E. Zarza, P. Nava, J. Langenkamp, E. Mandelberg. EUROTROUGH – Parabolic Trough Collector Developed for Cost Efficient Solar Power Generation. In: Proceedings of the 11th SolarPACES International Conference, Zurich, Switzerland, 2002.

[36] L. Valenzuela, R. López-Martín, E. Zarza, Optical and thermal performance of large-size parabolic-trough solar collectors from outdoor experiments: A test method and a case study. Energy 70 (2014) 456−464.
[37] Crane CO. Flow of fluids through valves, fittings and pipe. Metric Edition, Technical Paper No. 410M. Crane Company. New York, USA, 1982.
[38] F.P. Incropera, D.P. DeWitt, T.L. Bergman, A.S. Lavine. Fundamentals of Heat and Mass Transfer, 6ª ed. John Wiley & Sons. New York, USA, pp. 675–691, 2006.
[39] R.C. Spencer, K.C. Cotton, C.N. Cannon. A method for predicting the performance of steam turbine-generators… 16,500 kW and larger. Paper No. GER-2007C, Revision of ASME Paper No. 62-WA-209, General Electric Company. New York, 1974.
[40] M.J. Montes, A. Abánades, J.M. Martínez-Val, M. Valdés. Solar multiple optimization for a solar-only thermal power plant, using oil as heat transfer fluid in the parabolic trough collectors. Sol Energy 83 (2009) 2165–2176.
[41] M.J. Wagner, P. Gilman. System Advisor Model Documentation. Technical Manual for the Physical Trough Model. Technical Report NREL/TP-5500-51825. National Renewable Energy Laboratory. Golden, CO, USA, p. 63-73, 2011.
[42] K. Wilbert, J. Maulbetsch. Air-Cooled Condenser Design, Specification, and Operation Guidelines. Technical Report 1007688. Electric Power Research Institute (EPRI). Palo Alto, CA, USA, 2005.
[43] K. Merlin, D. Delaunay, J. Soto, L. Traonvouez. Heat transfer enhancement in latent heat thermal storage systems: Comparative study of different solutions and thermal contact investigation between the exchanger and the PCM. Appl Energy 166 (2009) 107-116.
[44] I. Perez, A. Lopez, S. Briceño, J. Relancio. National incentive programs for CSP – Lessons learned. Energy Procedia 49 (2014) 1869-1878.
[45] E. Rojas, R. Bayón. Storage material inventory for nocturnal rejection. WP2.2-Heat rejection via storage for nocturnal exhaust. WASCOP Project Report, 2016.
[46] Syntroleum Corporation. Low-Cost Phase Change Material for Building Envelopes. Technical report for US Department of Energy, contract No. DE-EE00003924, 2013.
[47] P. Tan, P. Lindberg, K. Eichler, P. Löveryd, P. Johansson, A.S. Kalagasidis. Effect of phase separation and supercooling on the storage capacity in a commercial latent heat thermal energy storage: Experimental cycling of a salt hydrate PCM. J Energy Storage 29 (2020) 101266.
[48] N.H. Chen. An explicit equation for friction factor in pipe. Ind Eng Chem Fundam 18(3) (1979) 296–297. http://dx.doi.org/10.1021/i160071a019
[49] A.M. Patnode. Simulation and Performance Evaluation of Parabolic Trough Solar Power Plants [PhD Thesis]. Solar Energy Laboratory, University of Wisconsin, Madison, USA, 2006.
[50] A. Stodola. Steam and Gas Turbines, Vol. 1. Peter Smith. New York, USA, 1945.